









The impact of wind-waves and sea level rise on the morphodynamics of a sandy estuarine shoal

J. Zheng^{1,2}  | H. Elmilady^{1,2,3}  | B.R. Rübke¹  | M. Taal¹  | Z.B. Wang^{1,2}  | B.C. van Prooijen²  | P.L.M. de Vet^{1,2}  | M. van der Wegen^{1,3} 

¹Deltares, Delft 2600 MH, P.O. Box 177, The Netherlands

²Faculty of Civil Engineering and Geosciences, Delft University of Technology, The Netherlands

³IHE-Delft Institute for Water Education, The Netherlands

Correspondence

J. Zheng, Deltares, P.O. Box 177, Delft 2600 MH, The Netherlands.
Email: jiechen.zheng@outlook.com

Funding information

Deltares; Rijkswaterstaat

Summary

Intertidal shoals are pronounced morphological features found in many estuaries worldwide. Apart from maintaining an ecologically unique intertidal environment, shoals also protect adjacent dyke systems by attenuating waves. The fate of sandy shoals under anticipated sea level rise (SLR) scenarios is underexplored.

The current research investigates the long-term morphodynamic evolution of estuarine sandy shoals under forcing by short fetch, locally generated wind-waves, tides, and SLR by means of a numerical, process-based model (Delft3D). The focus lies on a sheltered shoal complex in the Western Scheldt, the Netherlands. Starting from the initial, 1963 bathymetry, we model 50-year morphodynamic development with schematized wind-wave forcing. We analyze in detail the impact of locally generated wind-waves on shoal formation. Finally, we impose regional SLR of 1.10 m and 1.95 m for 100 years.

Model results show that, on the spatial scale of intertidal flats, small, locally generated wind-waves lower and widen the shoals while the adjacent channels deepen. However, on the estuarine system scale, wind-waves do not lead to fundamentally different channel–shoal patterns and morphodynamic evolution trends. This suggests that channel–shoal formation is mainly due to tide residual sediment transports, with wind-waves playing a secondary role. SLR leads to a notable intertidal area loss, despite a continuous heightening of the shoals, implying that morphodynamic adaptation lags behind SLR. The inclusion of wind-waves does not fundamentally change the reaction of the estuarine shoal to SLR. Future research may focus on exploring the impact of including multiple sediment classes.

KEYWORDS

Estuarine morphodynamics, Intertidal flat, Morphodynamic modeling, Sandy shoal evolution, Sea level rise

1 | INTRODUCTION

Estuaries are partially enclosed coastal bodies of water where rivers meet the sea. With their variations of water temperature, salinity, turbidity, and flow, estuaries provide unique habitats to a variety of flora and fauna (Do Ó Martins et al., 2020; Moyle et al., 2010). Estuarine shoals commonly emerge in sediment-rich environments. They often comprise intertidal areas that are flooded at high tide and exposed at

low tide. Once vegetated, this intertidal area provides vital habitats for a number of species, including salt marshes, mangroves, etc. (Ancora et al., 2020; Kwon et al., 2020).

The sedimentology and geomorphology of shoals are formed by hydrodynamic forcing conditions and the nature of the sediment supply. Sandy shoals are usually found in high-energy, sand-rich environments, whereas muddy shoals often emerge in sheltered, low-energy, mud-rich areas (Friedrichs, 2012). Fringing shoals exist along estuary

This is an open access article under the terms of the Creative Commons Attribution License, which permits use, distribution and reproduction in any medium, provided the original work is properly cited.

© 2021 The Authors. *Earth Surface Processes and Landforms* published by John Wiley & Sons Ltd.

boundaries, while other shoals exist in a free form surrounded by deep tidal channels (Hibma et al., 2004; Robinson, 1960).

In a tide-dominated, sandy estuary, typical morphological features are ebb and flood channels meandering between shoals (Ahnert, 1960; Robinson, 1960). The channel–shoal patterns arise from positive feedback between tidal currents, sediment transport, and initial bedforms (Hibma et al., 2004; Schramkowski et al., 2002; Schuttelaars & Swart, 1999; Seminara & Tubino, 2001), while the plan form of the estuary has an impact on their location and bar scales (Dam et al., 2016; Lanzoni, 2002; Van der Wegen & Roelvink, 2008, 2012).

The intertidal morphology is governed by a complex interaction between tidal hydrodynamics, wave action, and sediment supply (e.g., Friedrichs, 2012; Kirby, 2000; Le Hir et al., 2000; Roberts et al., 2000). Tidal forcing usually causes onshore sediment transport, while waves enhance shoal erosion and prevent deposition (Christie et al., 1999; Le Hir et al., 2000; Yang et al., 2003). In response to increased sediment supply and a large tidal range, convex-up cross-section profiles are likely to form, while concave-down profiles are associated with decreased sediment supply and increased wave action (Bearman et al., 2010; Friedrichs, 2012; Hunt et al., 2015). Wind-waves play an important role in morphodynamic states (Fagherazzi et al., 2007; Maan et al., 2018; Van der Wegen et al., 2016; Van der Wegen et al., 2019). High wave energy tends to generate a steeper intertidal profile (Roberts et al., 2000; Friedrichs, 2012). By studying the Dutch Wadden Sea and Eastern Scheldt, respectively, Janssen-Stelder (2000) and Koksiek et al. (1988) highlighted that a combination of tidal currents and wave action is responsible for the erosion of the intertidal flat during storm conditions. DeVet et al. (2018) showed that a sandy shoal may propagate along the wave direction and wind direction. Elmilady et al. (2020) highlight that wave-induced resuspension is essential for distributing sediment supplied from deep channels over the intertidal flat.

In recent years, process-based numerical models have become an increasingly popular tool and virtual laboratory to explore estuarine morphodynamic development. Examples are the evolution of channel–shoal patterns in schematized tidal basins (e.g., Hibma et al., 2004; Kleinhans et al., 2008; Van der Wegen & Roelvink, 2012; Wang et al., 1995; Zhou et al., 2015) or hindcasts and forecasts in more realistic environments (e.g., Arafat et al., 2016; Dam et al., 2016; Elmilady et al., 2019; Ganju & Schoellhamer, 2010; Luan et al., 2017). Other studies have focused on exploring morphodynamics of isolated tidal flats by using one-dimensional (1D) profile models (e.g., Maan et al., 2015; Van der Wegen et al., 2016; Zhou et al., 2015) or two-dimensional (2D) models (e.g., DeVet et al., 2018; Elmilady et al., 2020; Fagherazzi et al., 2007; Nguyen et al., 2011). These studies apply a numerical process-based model to study estuarine morphodynamic development and show its increasing potential and reliability.

Sea level rise (SLR) will potentially have considerable impacts on estuary morphodynamics. Recent studies applying morphodynamic numerical models for estuarine systems show that sea level rise can lead to noticeable intertidal area loss (e.g., Dissanayake et al., 2012; Elmilady et al., 2019; Mariotti & Fagherazzi, 2010; Van Der Wegen, 2013; Van der Wegen et al., 2016) and a steeper slope of tidal flats (Mariotti & Fagherazzi, 2010). SLR-induced increased water depth weakens wave action on channel bank, where sediment deposition is favored. Despite sedimentation, intertidal flats cannot

keep pace with an exponentially rising sea level, leading to a loss of intertidal area along with increasing inundation frequency (e.g., Elmilady et al., 2019; Elmilady et al., 2020; Ganju & Schoellhamer, 2010; Van Der Wegen, 2013; Van der Wegen et al., 2016). Van Goor et al., (2003), Lodder et al. (2019), and Elmilady et al. (2020) suggest that intertidal flats can be maintained under a limited, linear SLR after a decadal adaptation time during which intertidal area is lost. This maintenance only exists when the accretion rate of the intertidal flats reaches the SLR rate. This usually requires a long adaption timescale and depends strongly on the local conditions of tides, waves, and sediment supply (Elmilady et al., 2020; Van Goor et al., 2003).

This synopsis reveals some intriguing knowledge gaps. Tidal basin models covering a large domain often use a coarse resolution of above 100 m to save computation time (e.g., Dam et al., 2016; Hibma et al., 2004; Van der Wegen & Roelvink, 2008; Wang et al., 2007), whereas smaller tidal flat models have a much higher resolution of typically 10–50 m (e.g., DeVet et al., 2018; Maan et al., 2018). The coarse resolution could disregard the subgrid (wave) dynamics and morphological structure, while the higher resolution is time-consuming. In addition, while tidal flat models stress the importance of wind-waves, many tidal basin models do not include wave action to reduce modeling complexity and computation time (e.g., Dam et al., 2016; Van der Wegen & Roelvink, 2012; Wang et al., 2007) or include waves which only impact mud transport (Braat et al., 2017). Tidal flat models including waves focus on the mud, while many estuarine shoals are sandy (e.g., Western Scheldt (Robinson, 1960), Waddenzee (Wang et al., 2012), and the Dyfi Estuary (Brown & Davies, 2010)). Furthermore, many studies apply a schematized and simplified model setup (e.g., Braat et al., 2017; Van der Wegen & Roelvink, 2012), disregarding site-specific conditions such as dredging and disposal activities for navigational purposes. Finally, although sea level rise threatens the survival of estuarine shoals and flats, limited process-based morphodynamic modeling studies have considered the impact of wind-waves when investigating anticipated sea level rise scenarios.

2 | AIM AND APPROACH

This research aims to explore the impact of wind-waves on the long-term morphodynamic evolution of estuarine sandy shoals in a realistic setting including the impact of sea level rise.

We apply a 2D process-based numerical model (Delft3D) to simulate the evolution of a shoal complex located in the landward side of the Western Scheldt estuary (the Netherlands). First, we assess the skill of our model in simulating decadal morphological development in a complex estuarine environment by qualitatively comparing modeled and measured bathymetries. We then compare the modeled shoal evolution over 50 years with and without waves and investigate the underlying reasons for the morphological difference caused by waves. Finally, starting from the 2013 modeled bathymetry and keeping the same wave environment in each scenario, we perform a 100-year forecast by imposing different sea level rise rates and study the impact of wind-waves on shoal evolution under SLR.

3 | STUDY AREA

The Western Scheldt estuary (the Netherlands; Figure 1) is one of the youngest natural estuaries in Western Europe. The large estuaries and tidal basins in the Netherlands were formed around AD 200 (Bosboom & Stive, 2012). Storms, floods, subsidence, and a continuing small sea level rise led to a rapidly increasing size of the Western Scheldt in the late Middle Ages (Van der Spek, 1994). Over time, various smaller secondary embayments have been reclaimed, decreasing the area of the Western Scheldt and with some impacts on the morphology of the main channels (Dam et al., 2016; Nnafie et al., 2019). Nowadays, it is a funnel-shaped mouth of the River Scheldt. The tide propagates up to Ghent, which is located around 160 km upstream (Figure 1). Its cross-section width decreases roughly exponentially from the estuary mouth at Vlissingen (around 5 km wide) to the estuary head near Ghent (less than 100 m wide). The width-averaged depth decreases from about 15 m at Vlissingen to 3 m at Ghent. The morphology of the Western Scheldt is a multiple-channel system with ebb channels and flood channels separated by intertidal shoals (Van Veen, 1950). It is a sand-dominated estuary with less than 10% mud, mostly found alongside the estuarine margins and salt marshes (Kuijper et al., 2004). Major dredging activities have taken place since the 1970s to guarantee navigation to the Port of Antwerp (Vroom & Schrijvershof, 2015; Wang et al., 2002).

The estuary is a tide-dominant system that is subject to strong spring-neap tidal variations. The most dominant tidal components are semi-diurnal (M2) and quarterly diurnal tides (M4) (Wang et al., 2002). The mean tidal range is 3.8 m at Vlissingen, 5.2 m at Niel, and 1.9 m at Ghent, with ratios between the rising and falling durations of 0.88, 0.75, and 0.39, respectively. The annual-averaged discharge from the River Scheldt at the confluence of the Rupel and Scheldt amounts to about 110 m³/s. The yearly variation ranges from 50 to 200 m³/s (Kuijper et al., 2004). In the landward portions of the Western Scheldt,

local winds generate waves with an average significant wave height of 0.2 m, propagating mainly from the southwest, northeast, and northwest.

This study focuses on the shoal complex (right panel in Figure 1) including the Shoal van Ossensisse, the Molenplaat, and the Rug van Baarland located in the mid-estuary, about 30 km landward from the mouth. This area is chosen because it is subject to limited penetration by North Sea offshore waves, which allows for the implementation of a wave model covering a part of the inner estuary and only considering small locally generated wind-waves. Shoals and the adjacent channels in this area are sand dominated with D₅₀ ranging from 120 μm to 250 μm (Kuijper et al., 2004).

4 | MODEL CONFIGURATION

In this research, we apply a two-dimensional horizontal (2DH) Delft3D model to simulate the long-term morphological evolution of the Western Scheldt estuary. This is a coupled flow and wave model (Figure 1). The flow model solves the shallow water equation and includes morphodynamic changes. The sediment transport formula distinguishes suspended load transport and bedload transport according to a reference height (Van Rijn, 1993). The wind-generated waves are calculated by the spectral wind-wave model SWAN (Booij et al., 1999). This describes waves by the two-dimensional wave action density spectrum. The flow model is coupled to the wave model through online coupling and the calculation of the current-wave interaction. More descriptions of the model terminology are reported in the Supporting Information.

The implemented model configuration is based on the NeVla-Delft3D model, which is calibrated for hydrodynamic conditions (Maximova et al., 2009; Vroom et al., 2015) and has been previously used for morphodynamic investigations (Grasmeijer et al., 2013; Van

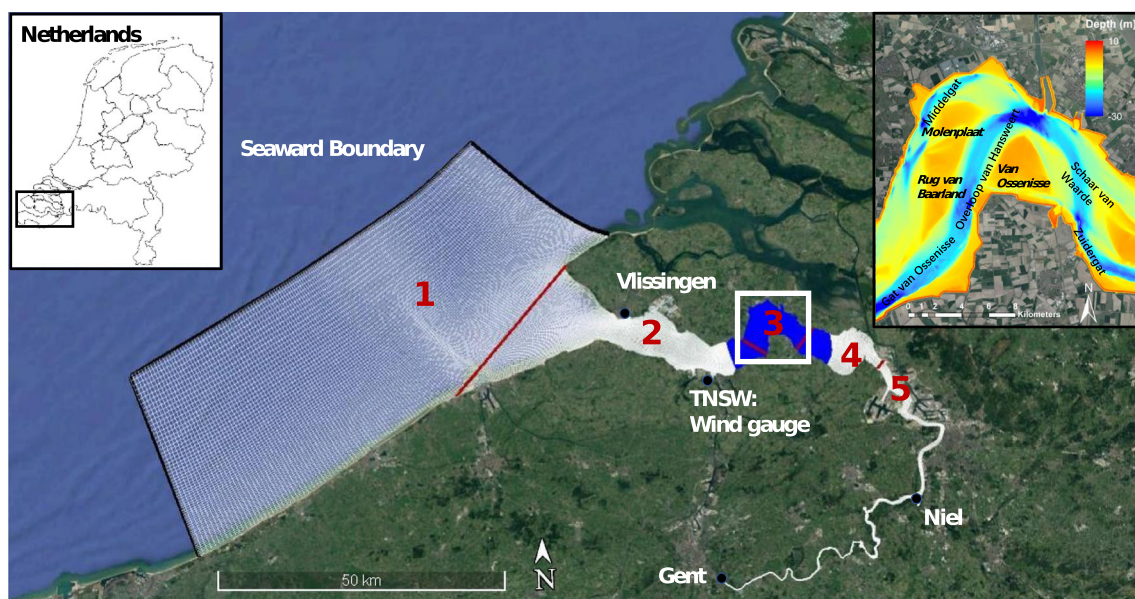


FIGURE 1 Google Earth image of the Western Scheldt estuary with the flow (white) and wave (blue) model computational domain plotted. Red lines indicate the division of five subdomains of the flow model. Wave model grids overlap flow domain 3 and extend to domain 2 and 4. The top left plot shows a map of the Netherlands. The top right plot is the bathymetry of the current study area in the year 1963. The bathymetry is with reference to NAP (Amsterdam Ordnance Datum), and 0 m refers to mean sea level (MSL). This datum is applied to the whole publication

der Werf & Brière, 2013; Van Dijk et al., 2019). Our model setup follows the work by Van der Wegen et al. (2016), who performed a morphological hindcast of the Western Scheldt (1963–2013) with an adjusted 2DH-NeVla-Delft3D model and carried out some preliminary sensitivity analysis. The model captures the evolution trend of the tidal amplitude. The amplitude difference of M2 tide at ten stations over 50 years shows values no more than 0.3 m. The model calculates the Brier skill score (BSS) over the whole estuary. Following the suggestion from Sutherland et al. (2075), the BSS is calculated to quantify the model skill using Equation 1. The skill score shows that the landward part performs better than the wider mouth and about 45% of the modeled erosion and sedimentation volume in the landward domain meets the criterion $BSS \geq 0.5$.

$$BSS = 1 - \frac{\langle (\Delta vol_{mod} - \Delta vol_{meas})^2 \rangle}{\langle \Delta vol_{meas}^2 \rangle} \quad (1)$$

in which Δvol is the volumetric change compared with the initial bed (m^3), mod is the modeled quantity, meas is the measured quantity, and brackets denote the arithmetic mean.

We implement a 2D model approach instead of a three-dimensional (3D) model due to computational time limitations. The work by Van der Wegen et al. (2016) on this configuration includes a 3D model run and carries out a comparison between the 2D and 3D models. Although the 3D model shows more diffuse patterns and more bent channels, it does not lead to a significant improvement. The 2D model is adequate to reproduce the channel–shoal evolution over the 50 years (1963–2013). Moreover, Van der Wegen and Roelvink (2012) perform extensive comparisons while reproducing the Western Scheldt starting from a flat bed for hundreds of years. The 2D morphological model shows the capability to capture the evolution and allocation of channel–shoal patterns and longitudinal profiles. In addition, the Western Scheldt estuary is well mixed and the 2DH model for suspended sediment transport in Delft3D is a quasi-3D model (Galappatti & Vreugdenhil, 1985; Wang, 1992).

We divide the NeVla flow model grid into five subdomains to allow for parallel processing and local grid refinement. The seaward boundary extends 20 km from the estuarine mouth while the landward riverine boundary is located in Ghent, Belgium. Domain 3 (Figure 1), where our studied shoal complex is located, has an average resolution of around $40 m \times 40 m$. The other four domains have a grid that is relatively coarser by a factor of 2. The total number of cells in the flow grid is 46,434. The high-resolution wave grid has an average resolution of around $40 m \times 40 m$ covering flow domain 3 and extending around 5 km into its adjacent domain 2 and domain 4.

The seaward flow model boundaries are prescribed with water levels. The boundary conditions are generated by nesting the Western Scheldt grid into the Delft3D Flexible Mesh Global Tide and Surge Model (GTSM) (Verlaan et al., 2015). To carry out sea level rise scenarios, we forced the GTSM model with 100-year global mean sea level rise (GMSLR) of 0.96 and 1.67 m, representing the 50th percentile of RCP 4.5 and 8.5 projections, respectively, by Le Bars et al. (2017). Derived from GTSM, the GMSLR results in a regional SLR of 1.10 m and 1.95 m, respectively, after 100 years (2113) at our seaward boundary. For each of the two scenarios, we prescribe two types of rising signal, viz. linear and exponential (referred to as nonlinear throughout the whole paper); see Figure 2b for an example

of the 1.10 m SLR. The landward boundary conditions prescribe constant discharges at two locations. One is $10 m^3/s$ from Niel, Belgium, and the other is $5 m^3/s$ from Ghent (sensitivity analysis shows that variation of the river discharge in a reasonable range does not cause a notable difference on the estuarine morphological evolution). Equilibrium sand concentrations are applied at all boundaries.

The initial bed level is the observed bathymetry of the year 1963 and consists of sand. Following Dam (2013), we applied nonerodible layers representing Pleistocene deposits and peat layers throughout the model domain. Extensive dredging and disposal events have taken place in the Western Scheldt since the 1970s (the polygons and time-series dredging events are presented in Section 5 of the Supporting Information). These are also included in our model by defining dredging and disposal polygons in which a time-varying minimum depth is maintained. Once, during a morphodynamic run, the bed level in a cell exceeds this depth, the bed level is reduced while the sediment is deposited at another predefined location, following historical dredging strategies (Vroom & Schrijvershof, 2015).

We analyzed wind data from 1999 to 2017 with 10-min intervals at Terneuzen Port (TNWS; Figure 1) to schematize the wind climate at the shoal complex. The constructed wind rose (Figure 2a) clearly shows that the dominant wind direction is southwest, accounting for 57% of the time, while the secondary wind directions are northeast and northwest, accounting for 26% and 17.53%, respectively. All simulations include wind forcing but from different directions, i.e., southwest, northeast, and northwest, with the same constant wind speed of 5 m/s. Simulations with waves turn on the wave module and generate waves with a maximum H_s less than 0.25 m.

We use a morphological factor to accelerate the morphological modeling. Based on sensitivity analysis by Van der Wegen et al. (2016), a value of 104 is determined. Other implemented model settings and parameters are presented in Table 1. This modeling configuration takes about 3 days to simulate 6 months of hydrodynamic time on an eight-core (2.6 GHz) machine.

5 | MODEL RESULTS

5.1 | Observed and modeled morphological development

We assess the model results over the whole estuary by visually examining the modeled and observed bathymetry after 50 years (2013; Figure 3b and 3c) along with the sedimentation/erosion patterns during the period (1963–2013; Figure 3d and 3e). Applying a similar process-based modeling approach (based on the NeVla model) in the Western Scheldt, Dam et al. (2016) suggest that the model skill is initially weak but increases after decades. The model bathymetry initially adapts to the schematized and limited model parameter settings, after which the cumulative effect of the main governing process eventually becomes more pronounced and the model captures the more realistic morphodynamic developments. In the Western Scheldt, the governing process is directed by the interaction of tidal forcing and estuarine geometry (Wang et al., 2002).

Figure 3 shows that the model skill varies over the domain. In general, the modeled bed level changes are larger than the observed changes. The model results show more deposition in the seaward

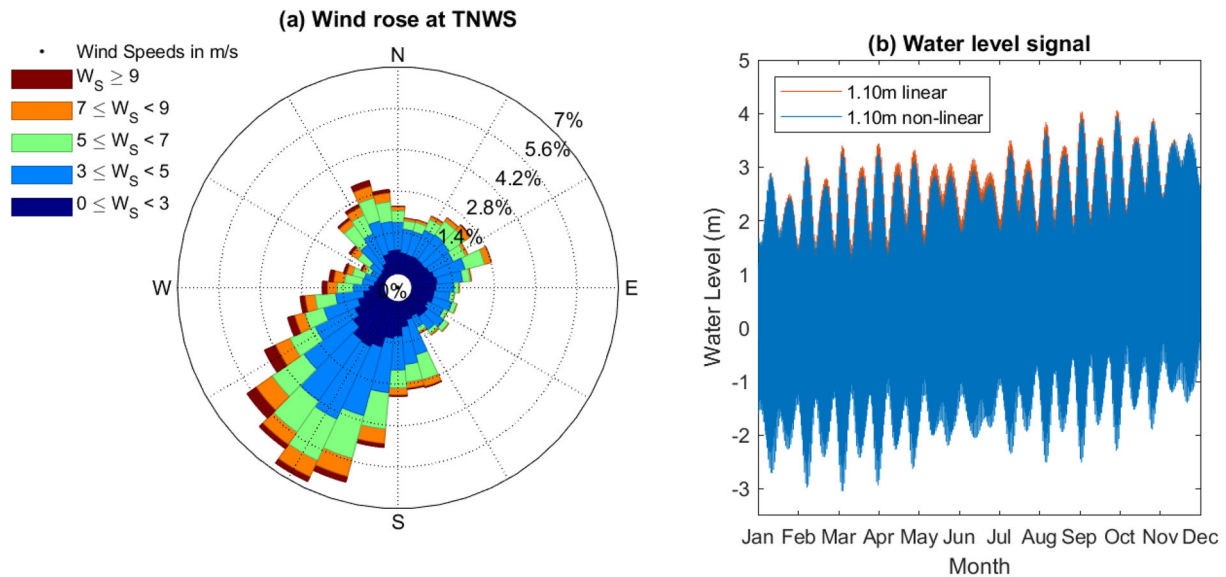


FIGURE 2 (a) Wind rose at station TNWS constructed from data from years 1999 to 2017, which shows wind directions are mainly from the southwest, along with northeast and northwest as secondary directions. (b) Water level signal on the seaward boundary for SLR of 0–1.10 m nonlinear versus SLR linear. Water level signal for SLR 0–1.95 m nonlinear versus linear is plotted in Supporting Information

TABLE 1 Additional model parameters

Parameter	Value
Time step	15 s
Hydraulic forcing	Water levels nested from GTSM model
Wave communication interval	60 min
Sediment transport formulation	Van Rijn 1993
Sand diameter (D_{50})	180 μm
Transverse bed slope factor (Abn)	60
Roughness	Spatially varying Manning (0.017 to 0.028 $\text{s/m}^{1/3}$)
Hydraulic runtime	73 days
Morphological factor (MorFac)	104
Morphological runtime (standard runs)	50 years (1963–2013)
Morphological runtime (SLR runs)	100 years (2013–2113)

portion of the estuary compared with observations. One of the reasons may be that our model does not include waves originating from the sea. The pronounced sedimentation on Shoal Hoogeplaten (from x-coordinates 30 to 40 km compared between Figure 3d and 3e) is overestimated because this is a disposal location for dredged material. The disposal algorithms of dredged material are rudimentarily implemented in the model and may not reflect detailed and actual disposal processes (timing, quantities, locations, and dumping directly on the bed instead of releasing dredged material at the water surface). Also, the absence of wave-induced shear stresses limits the resuspension of the dumped sediment in the seaward portion.

Modeled sedimentation and erosion patterns in the landward estuary section show a greater resemblance to observations.

Considerable prescribed dredging activities in the channels play an important role in this. The model performs well at Shoal Molenplaat (see Figure 1 for shoal names) and reflects the sedimentation and erosion in the nearby channels. Shoal van Ossensisse is relatively stable, as in reality. An observed difference is that the northern side of the shoal edge is more flattened in the model. The implemented schematized model settings are factors that contribute to the difference between model results and observations, for example, a single sediment fraction and a schematic model roughness representation. In particular, we calculate the BSS value in domain 3 (Figure 1), which is 0.14 and considered as reasonable (0.1–0.3) according to the BSS rating for morphological models.

The aim of the current work is not to reproduce observed developments but rather to explore the impact of wind-waves on morphodynamic development. We consider the model accuracy to be high enough and to generate a stable morphology in the surroundings of Shoal van Ossensisse to continue exploring the impact of wind-waves on morphodynamic development.

5.2 | Impact of wind-waves on shoal evolution

We investigate the impact of wind-induced waves on the intertidal area by comparing simulations with waves (Wave) and without waves (NoWave). Figure 4 shows the bathymetry difference (Wave – NoWave) over 50 years when applying different wind directions. Red/blue color indicates a higher and lower bed level for the Wave than NoWave case. Note that higher/lower bed level can be due to more/less sedimentation or less/more erosion for the Wave than NoWave case. Focusing on Shoal van Ossensisse and the simulation with the dominant wind direction 207° (first column of Figure 4), Figure 4a shows that waves start to erode the high sections of the shoal and the upwind intertidal area immediately after 10 years, as indicated by the blue color at the top of the shoal. More sediment occurs at shoal edges (red color) and the downwind side of the shoal.

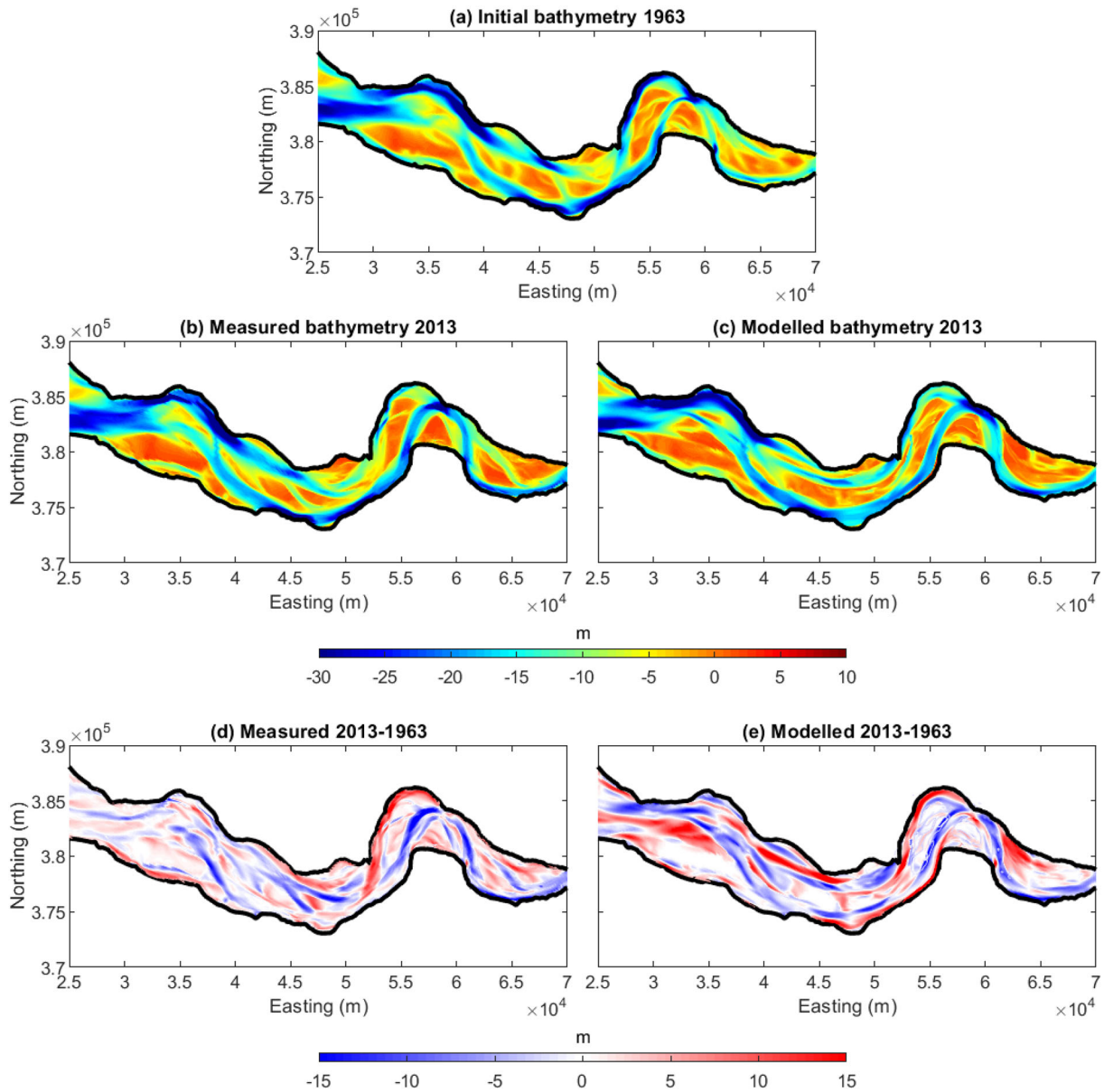


FIGURE 3 (a) Initial bathymetry. (b) Measured and (c) modeled bathymetry after 50 years (2013). (d) Measured and (e) modeled cumulative erosion and sedimentation patterns between 1963 and 2013

Channels become deeper, mainly in places where shoal edges gain more sediment.

The developments are cumulative in the sense that initial differences only increase over time and do not evolve to fundamentally different patterns (see Figure 4b for $T=30$ and Figure 4c for $T=50$). The difference in bathymetry can be up to 3 m after 50 years. These trends can also be observed in other wind direction scenarios (second column of Figure 4 for wind direction 70° and third column of Figure 4 for wind direction 304°). Furthermore, we observe that the shoals show a tendency to migrate slightly along the direction of wave propagation. There appears to be a slight difference in the trend at the location (around $x=6.0 \times 10^5$ m, $y=3.82 \times 10^4$ Åž,m) for wind direction from 340° . This is because of the curved meandering location with a complex flow situation.

Measured intertidal area (Figure 5a) and intertidal volume (Figure 5b) increase in the 1970s followed by a stabilization. This is similar to the modeled behavior, although the model results underestimate the intertidal volume by about 16%. The considerable rise of the

intertidal area and volume in the 1980s is mainly due to the disposal of dredged material on channel banks as reflected by large, sudden shifts in values. After 2000, the modeled channels are no longer much affected by major dredging operations. Wave cases show a slightly larger intertidal area and volume than the NoWave cases (about 5%) throughout the last 20 years.

Measured and modeled channel area (Figure 5c) and channel volume (Figure 5d) initially decrease, followed by an increase since the 1990s. This implies that the channel experiences a period of sedimentation followed by erosion. The model captures this trend with similar magnitudes. The impact of waves is limited and leads to a slightly narrower channel area, while the channel volume does not differ greatly from the NoWave simulations. Less channel area is associated with a larger intertidal area with waves (Figure 5a). Initially, the Wave cases show slightly higher channel volumes. Afterwards, the difference minimizes and almost vanishes at the end.

The hypsometric curve shows the percentage of area below a certain bed level and is used to characterize the morphological state of

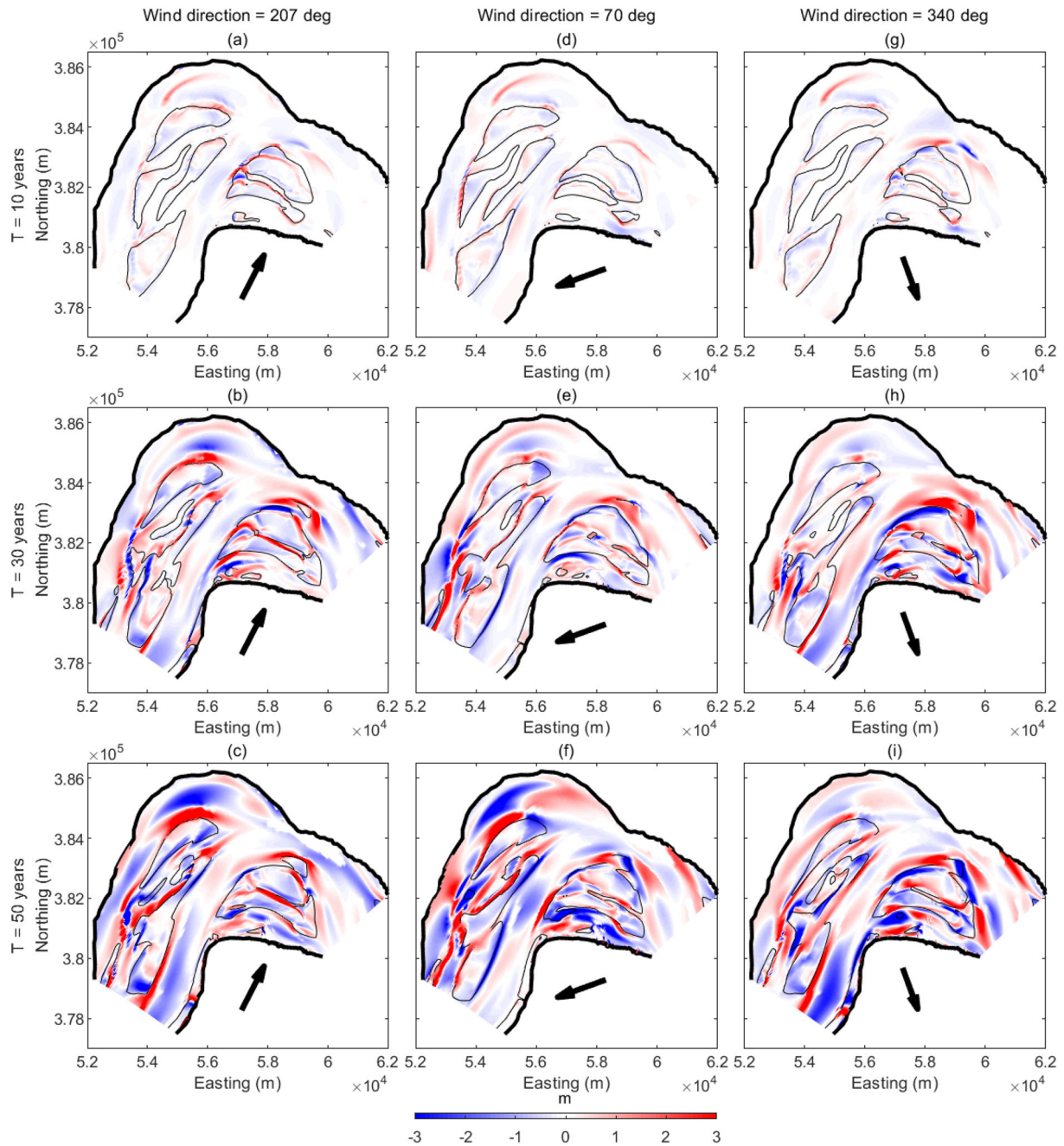


FIGURE 4 Bathymetry difference (Wave - NoWave) along time (row 1: after 10 years; row 2: after 30 years; row 3: after 50 years) for different wind directions. Column 1: direction 207°; Column 2: direction 70°; Column 3: direction 340°. Red colors indicate more sedimentation or less erosion in the Wave case; blue colors represent less sedimentation or more erosion in Wave case. The thin black line is the -2.3 m contour line of the NoWave case in the year 2013. The black arrow indicates wind direction

an estuary (Boon, 1975). Figures 6a, 6c, and 6e show the hypsometry of the study area, while Figure 6b, 6d and 6f show the difference between the Wave and NoWave simulations (Wave - NoWave), in which positive/negative values imply lower/higher elevation in the Wave compared with NoWave case.

In general, the hypsometry of Wave and NoWave cases are close, and their area percentage difference does not exceed 3% over the whole modeling period. Nevertheless, waves still have a persistent influence. After 10 years, in Figure 6b, we observe a positive value above MSL, which means that the shoal elevation above MSL is lowered by waves. Simultaneously, widening of the area appears at the lower intertidal region (between around -1.8 m to 0 m) and upper subtidal region (between around -5 m to -1.8 m).

This corresponds to the larger intertidal area in the Wave cases calculated in Figure 5a. In the meantime, below -10 m, the channel becomes deeper and wider. These trends become more pronounced over time (see $T=30$ in Figure 6c and 6d and $T=50$ in Figure 6e and 6f). Consequently, the combination of a narrower channel area right below MLLW (around (-1.8 m) to (-10 m) MSL) and a wider area at the lower part of the channel (below -10 m MSL) in Wave cases results in a relatively constant channel volume difference (Figure 5d).

Different wave direction scenarios show similar trends. In summary, Figure 7 shows a schematized representation of the impact of waves on the cross-sectional profile. The top of the shoal is lowered with larger intertidal area and upper subtidal area, while the channel is

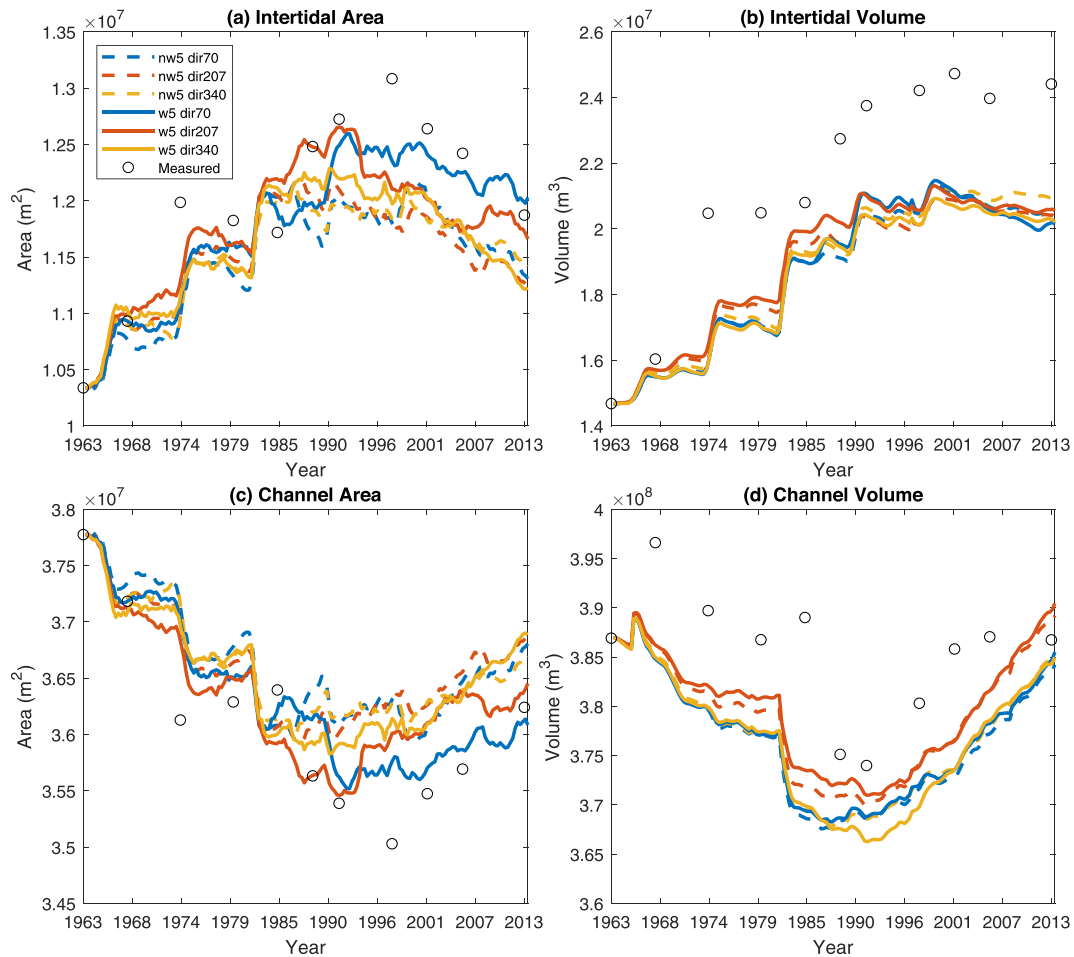


FIGURE 5 Development over 50 years of (a) intertidal area, (b) intertidal volume, (c) channel area, and (d) channel volume. Dash lines indicate the NoWave case; solid lines with the same color indicate the Wave case in the same wind condition. Values are calculated in the the study area including Shoal van Ossensisse, the Molenplaat, and the Rug van Baarland. The border between the intertidal section and the channel is defined at the averaged mean low low water (MLLW) which is -1.8 m below mean sea level (MSL)

wider at larger depths (below around -10 m) and deeper in the bottom.

5.3 | Processes underlying wind-wave impact

In this section, we substantiate an explanation for the elevation lowering and widening of the intertidal area along with the channel widening and deepening at large depths. We hypothesize that waves erode the intertidal area by enhancing the bed shear stress on the shoal. This raises suspended sediment concentrations in the water column at the shoal. Combined with wave asymmetry and wind-driven flow, a high SSC enhances sediment transport from the shoal towards the channel in the direction of wave propagation and causes higher prevailing SSC on the leeside of the shoal. In addition, increased SSC levels will occur at the shoal edges by ebb currents draining the shoal. As a result, the shoal widens and the channel narrows. This leads to flow convergence and erosion in the channel with higher velocities, deepening the channel.

To investigate the sediment transport variation due to waves, we ran scenarios on a fixed bathymetry (without morphodynamic updates). Model results show that intratidal variations (from Supporting Information, Figure 2h) of the bed shear stress and SSC

have peaks when the water level is around MSL. At this stage, the large flow velocity enhances nonlinear wave-current interactions, increasing bed shear stress and inducing high SSC, especially on the upwind side. During low water slack, the influence of waves can be extended to the subtidal domain, but the amount of area feeling wave motion is limited. During high water slack, the water depth is too large, so that the bed level hardly feels wave motion anymore.

Figure 8 shows the tidal inundation-averaged, wave-induced bed shear stress for different wind direction scenarios. In the case of a wind direction of 207° (Figure 8a), relatively high bed shear stresses occur on the upwind side of the shoal by a high significant wave height. High bed shear stress also occurs over the shoal in areas with elevation above MSL. This is because the high-elevation section experiences a short inundation duration. Different wind directions show similar observations (Figure 8b and 8c). The magnitude for the direction 207° is higher than that for other directions because it has a longer fetch, hence leading to higher waves.

Waves hardly affect the flow patterns (Figure 9a), in terms of either magnitude or direction. Some insignificant change is due to Stokes drift in the direction of wave propagation, mainly occurring in the lower intertidal area with high significant wave height.

However, waves considerably alter the suspended sediment transport over the entire shoal (Figure 9b). As discussed above, waves

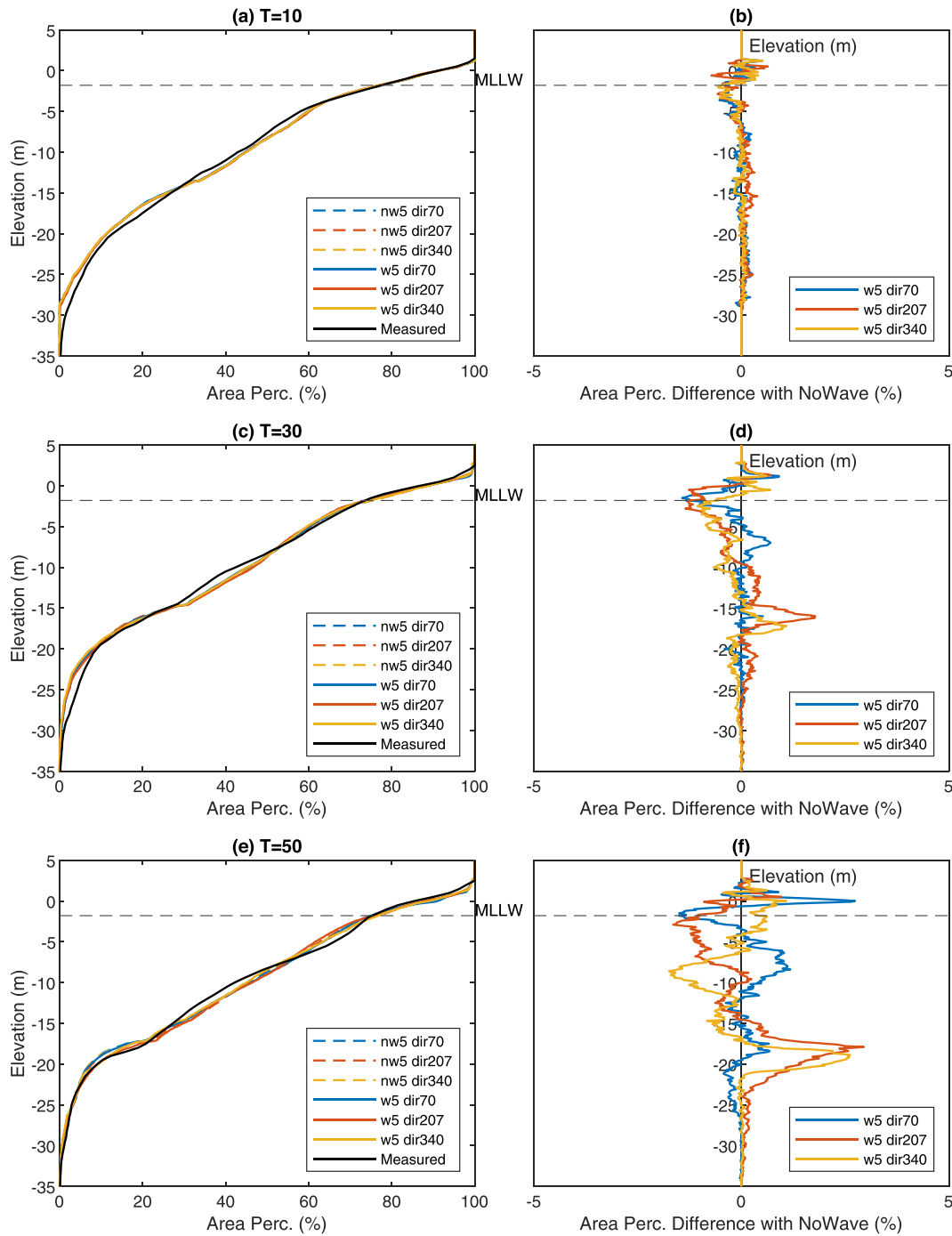


FIGURE 6 Hypsometry along time. (a, c, e) Hypsometry for all scenarios: dashed line indicates the NoWave case, solid line with the same color indicates the Wave case in the same wind condition; (b, d, f): Area percentage difference between Wave and corresponding NoWave case. Positive values imply lower elevation in the case of Wave compared with NoWave

induce more SSC in the water column. On the one hand, high SSC is transported by wind-driven flow along the wind direction from the upwind side and settles in the leeside. On the other hand, high SSC is transported by ebb tidal currents towards the channel, where the sediment settles at locations of low bed shear stress. As a result, we observe more sediment at the leeside and submerged edges of the shoal (Figure 4).

Tidal residual bedload sediment transport is more directed towards the wave propagation direction (Figure 9c). This is because, in Delft3D, the bed load transport equation includes the suspended sediment transport caused by wave asymmetry, which represents a large portion of the total bedload sediment transport over the shoal.

However, the bedload sediment transport magnitude is negligible compared with the suspended sediment transport magnitude and barely contributes to the total sediment transport.

The scenarios with different wind directions all show that the Wave cases have larger flow velocities in the channel (Figure 10), especially near the areas of wider shoal edges caused by waves. This is because the flow converges in the channel due to the shoal widening. This adaption leads to local channel erosion. However, it does not change the estuarine channel evolution in the whole system. It can also be seen from the channel volume development (Figure 5d), where the difference in channel volume between Wave and NoWave cases initially deviates and becomes constant after about 25 years.

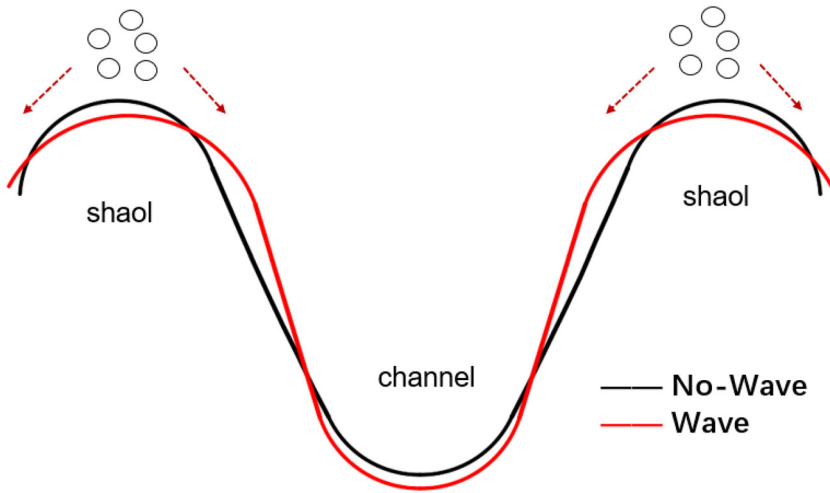


FIGURE 7 Schematic diagram of wave impact on cross-section channel-shoal profile: black line is the NoWave case; red line is the Wave case. Wind-waves lower and widen the intertidal area, with the adjacent channels deepening

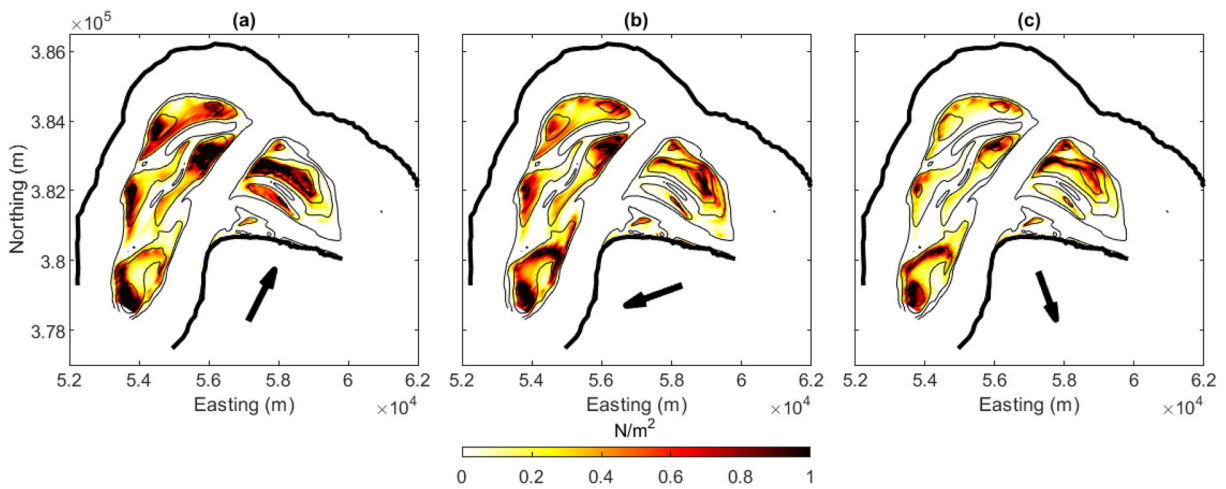


FIGURE 8 Tidally averaged wave-induced bed shear stress under inundation duration at the intertidal area: (a) direction 207°, (b) direction 70°, and (c) direction 340°. Black arrow indicates wind direction. The wave-induced shear stress is roughly calculated by the difference between the maximum bed shear stress and tide-induced bed shear stress from the model output

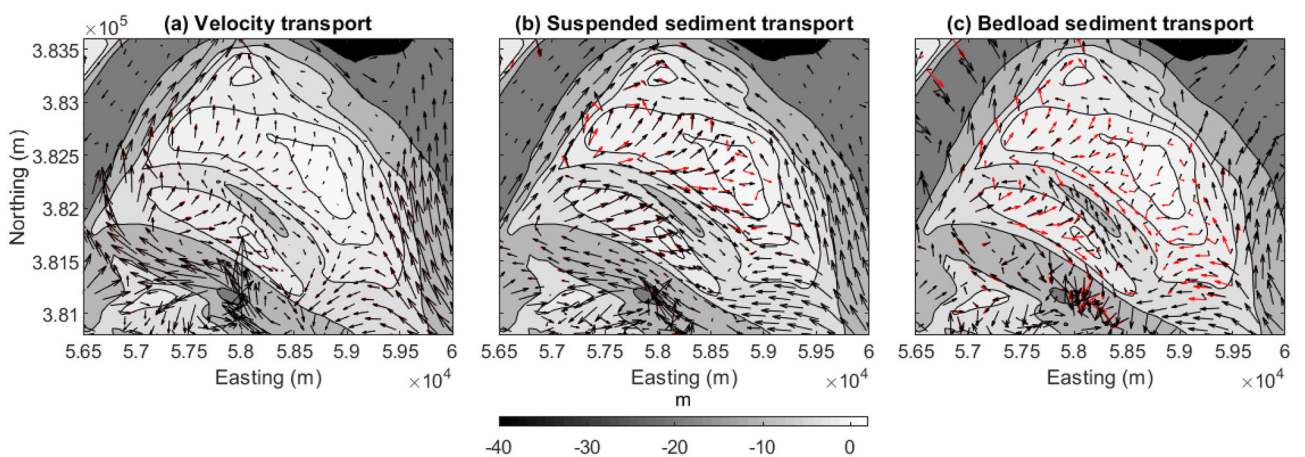


FIGURE 9 For wind direction 207°: (a) tide residual flow pattern, (b) suspended sediment transport pattern normalized by averaged magnitude over its root-mean-square (RMS) value per cell over one tidal cycle, and (c) bedload sediment transport pattern normalized by averaged magnitude over its RMS value per cell over one tidal cycle. White to black patches indicate the bed level. Black and red arrows indicate the transport direction of Wave and NoWave cases, respectively

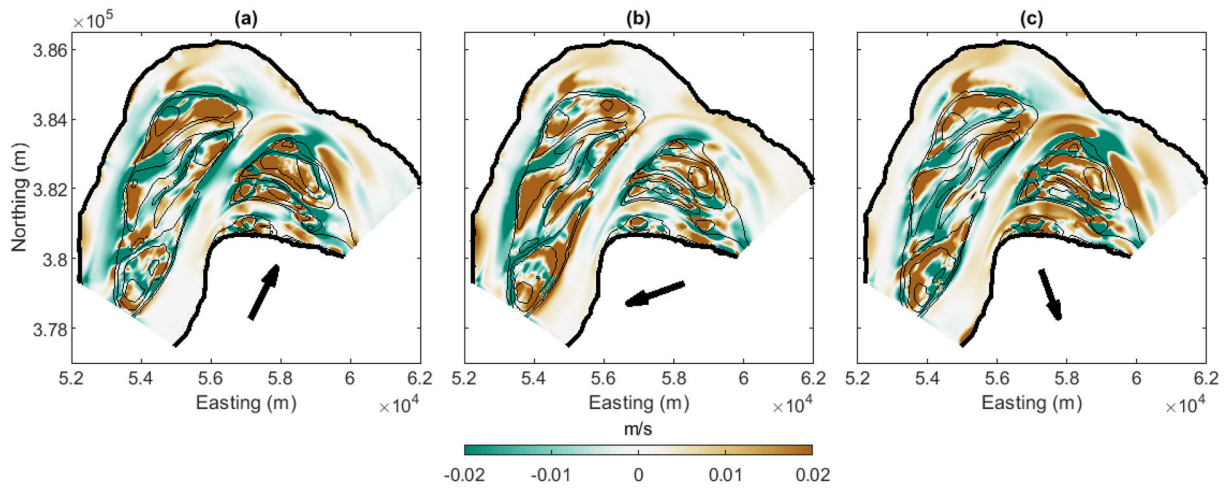


FIGURE 10 Difference (Wave - NoWave) of mean velocity magnitude over one tidal cycle after 5 years morphological change. Brown color indicates a larger magnitude in the case of waves: (a) direction 207°, (b) direction 70°, and (c) direction 340°. Black arrow indicates wind direction

TABLE 2 Overview of SLR simulations

Scenario	Wave/NoWave	SLR	Rising signal
S1	Wave	0 m	-
S2	Wave	0 to 1.10 m	Linear
S3	Wave	0 to 1.10 m	Nonlinear
S4	Wave	0 to 1.95 m	Linear
S5	Wave	0 to 1.95 m	Nonlinear
S6	NoWave	0 m	-
S7	NoWave	0 to 1.10 m	Linear
S8	NoWave	0 to 1.10 m	Nonlinear
S9	NoWave	0 to 1.95 m	Linear
S10	NoWave	0 to 1.95 m	Nonlinear

5.4 | Sea level rise impact on shoal evolution

Starting from the 50th year morphological state generated in Section 3, we performed 100-year runs while imposing SLR scenarios at the model seaward boundaries, under no wave (NoWave) and wave (Wave) conditions. There is one scenario with no SLR (NoSLR) plus four SLR scenarios (SLR) with SLR of 0 to 1.10 m (moderate case) and 0 to 1.95 m (extreme case) in 100 years, with each having a signal of linear and nonlinear SLR rate. Due to computational time limitations, only wind from direction 207° is considered since this is the prevailing direction. All the scenarios are summarized in Table 2. Dredging and disposal events are continuous, with present strategies. The calculations of intertidal area and volume (> MLLW) and channel area and volume (< MLLW) are based on the rise of MLLW under SLR.

The 100-year SLR leads to noticeable shoal pattern variations in Shoal van Ossensisse, the Molenplaat, and the Rug van Baarland (Figure 11a, 11c, 11b, and 11d only show the SLR of 1.10 m nonlinear as a demonstration). Figure 11e and 11f show that SLR leads to more sediment at the upper channel bank and at the top of the shoal and notably impacts the shoal location. Comparing shoal patterns between NoWave and Wave in both NoSLR (Figure 11a and 11b) and SLR (Figure 11c and 4d) shows that the wave impact on shoal patterns becomes more pronounced in the following 100 years. In particular,

the prescribed single wave climate causes continuous shoal migration in the downwind direction (Figure 11g). The SLR scenario sees faster propagation due to wave actions (cf. Figure 11g and 11h, which show more sediment at the shoal leeside in Wave when imposing SLR 1.10 m). This is consistent with Elmilady et al. (2019), who showed that, as SLR increases the water depth on the shoal, the shallower area of the shoal starts to experience greater wind-wave influence. This increases the landward extent of wave attack on the upwind side and therefore sediment on the downwind side.

The study area experiences net erosion with a slightly increased channel volume and a decreased intertidal area and intertidal volume over 100 years (Figure 12). Figure 12e shows that SLR enhances the decrease of the total sediment volume, but the decrease is not a linear function of SLR rate and the trend line is not smooth but rather irregular and sometimes shockwise. For example, in NoWave cases, linear and nonlinear 1.10 m SLR, linear and nonlinear 1.95 m SLR lead to 9%, 47%, 62%, and 91% more erosion than NoSLR with respect to the initial state, respectively. Figure 12a shows an overall decrease of the intertidal area in the estuary. The development of the intertidal area does not keep pace with the rising sea level due to the SLR-induced increased inundation. The higher the sea level rise, the greater the decrease of the intertidal area. The nonlinear and linear SLR signals show a small difference. Initially, the decrease of intertidal area for nonlinear SLR signal is milder. Afterwards, the decrease rate becomes larger due to the faster inundation rate. Similar to the intertidal area, SLR causes a notable drop in the intertidal volume (Figure 12b), while the decrease does not linearly relate to SLR rate. A significantly larger channel volume (Figure 12c) by about 13% and 23% compared with NoSLR arises from 1.10 and 1.95 m SLR, respectively, by 2100. This is partly because of the increase in the inundated area below MLLW. Additionally, the channel volume calculated below the constant initial MSL (Figure 12d) suggests that SLR causes net erosion of the channel with a percentage of around 3% and 7% larger than NoSLR for the signal with 1.10 and 1.95 m.

The impact of waves does not differ much among the different SLR scenarios. Compared with the SLR impact, the difference in channel volume due to waves (less than 1%) remains limited. This implies that the magnitude of wave impact is much less than the magnitude

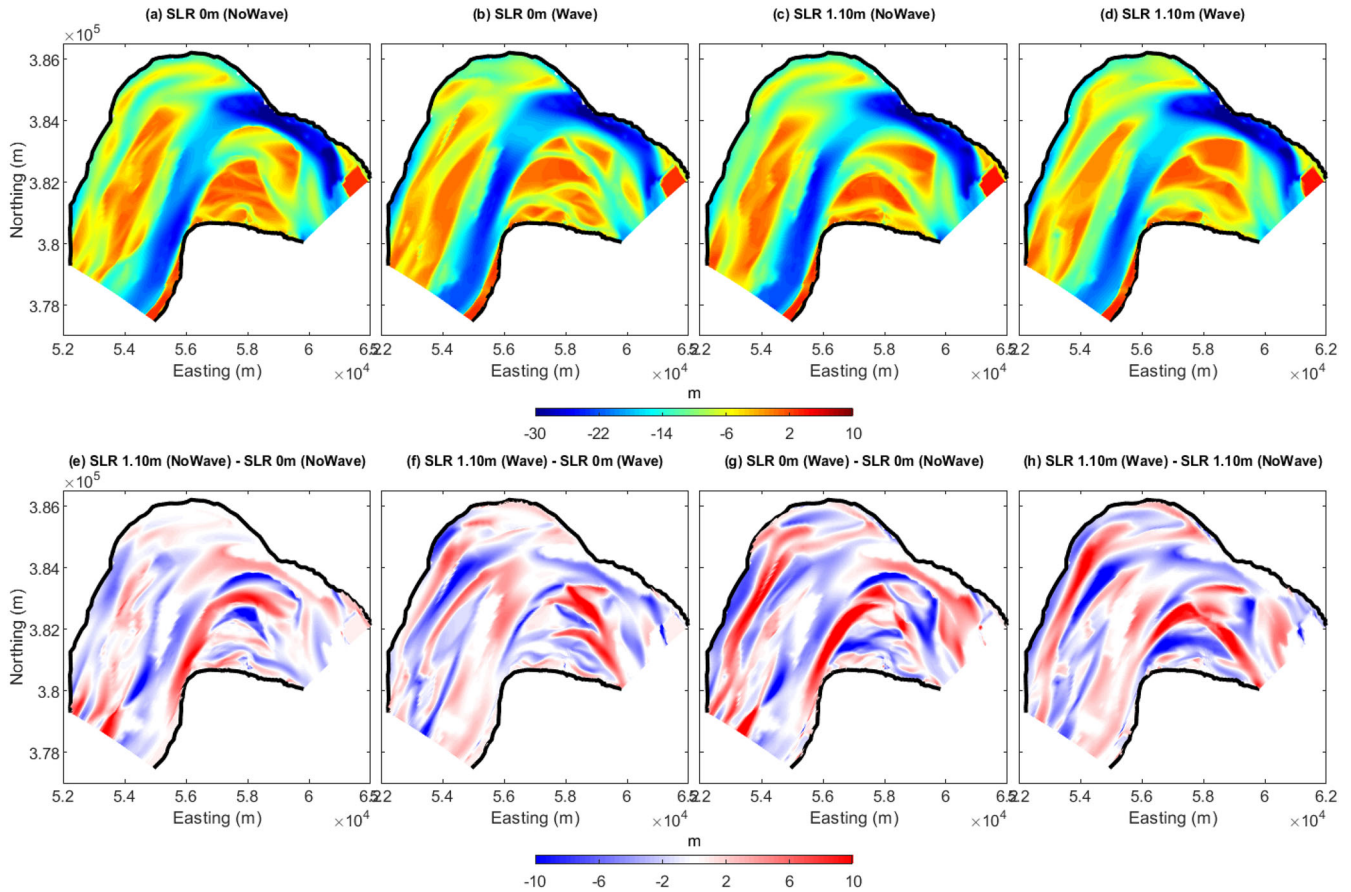


FIGURE 11 Bathymetry after 100 years of (a) SLR 0 m without wave, (b) SLR 0 m with wave, (c) SLR 1.10 m non-linear without wave, and (d) SLR 1.10 m nonlinear with wave. Bed levels are with respect to constant initial mean sea level (MSL). Bathymetry difference after 100 years of (e) SLR 1.10 m nonlinear without wave minus SLR 0 m without wave; (f) SLR 1.10 m nonlinear with wave minus SLR 0 m with wave; (g) SLR 0 m with wave minus SLR 0 m without wave; (h) SLR 1.10 m nonlinear with wave minus SLR 1.10 m nonlinear without wave

of SLR impact on the morphological development on a long timescale. Moreover, waves do not seem to fundamentally change the morphological response of the system to SLR.

Figures 13a and 13b illustrate the hypsometry difference between SLR and NoSLR after 100 years in the case of Wave and NoWave, respectively. Both of them show that the elevation of the top of the shoal increases with SLR and the shoal edges (above about -1.8 m with respect to constant initial MSL) gain sediment. However, the sediment trapping lags behind SLR and results in an overall drop of the intertidal area, as shown in Figure 12a. SLR widens the channel significantly, mostly between -2 m and -15 m (with respect to constant initial MSL). The hypsometry difference with NoSLR can be up to 7% for nonlinear SLR of 1.95 m. This is reflected in the greater channel volume due to SLR in Figure 12c. Comparing Figure 13a with 13b shows that including or excluding waves leads to similar trends and behavior of morphodynamic depth variations, although magnitudes may differ per scenario.

6 | DISCUSSION

On the spatial scale of intertidal flats, waves cause noticeable differences in intertidal morphological evolution over the decadal timescale. Despite the shoal accretion due to estuary evolution, waves show a persistent influence in eroding the intertidal sediment. Waves lead to

a lower elevation on top of the shoal compared with the NoWave situation and show a high eroding power at the upwind side of the shoal. This agrees with Fagherazzi et al. (2007) and Maan et al. (2018), who found that the morphological evolution of the intertidal area is a function of the shear stress caused by waves. Wave-induced suspended sediments are transported by tidal currents, leading to a net seaward transport (Janssen-Stelder, 2000; Elmilady et al., 2020). In our model, sediment transported from the shoals favors deposition in nearby areas where low bed shear stress exists, such as intertidal edges, widening the pronounced larger intertidal area. This effect is more pronounced for a smaller sediment grain size. Figure 14b shows that the shoal with a smaller sand grain size of 160 μm compared with 180 μm has a lower intertidal elevation (positive value for the blue line around shoal-top elevation level) but a larger area at shoal edges (negative value for the blue line around MLLW). The shoal with a larger sand grain size of 200 μm compared with 180 μm shows the opposite situation. This is because finer sand has lower critical shear stress for erosion and favors settling in shallower locations. Higher wave energy has a larger erosion impact (Figure 14d). This results in a lower averaged intertidal height and more sediment appearing at the edge of the shoal. In addition, the presence of waves increases the spatiotemporal morphodynamics of the intertidal flats. Research by de Vet et al. (2020) on temporal variations in wave climate (i.e., storm events) even shows that the irreversible morphological evolution of intertidal flats can be driven by waves combined with other hydrodynamic

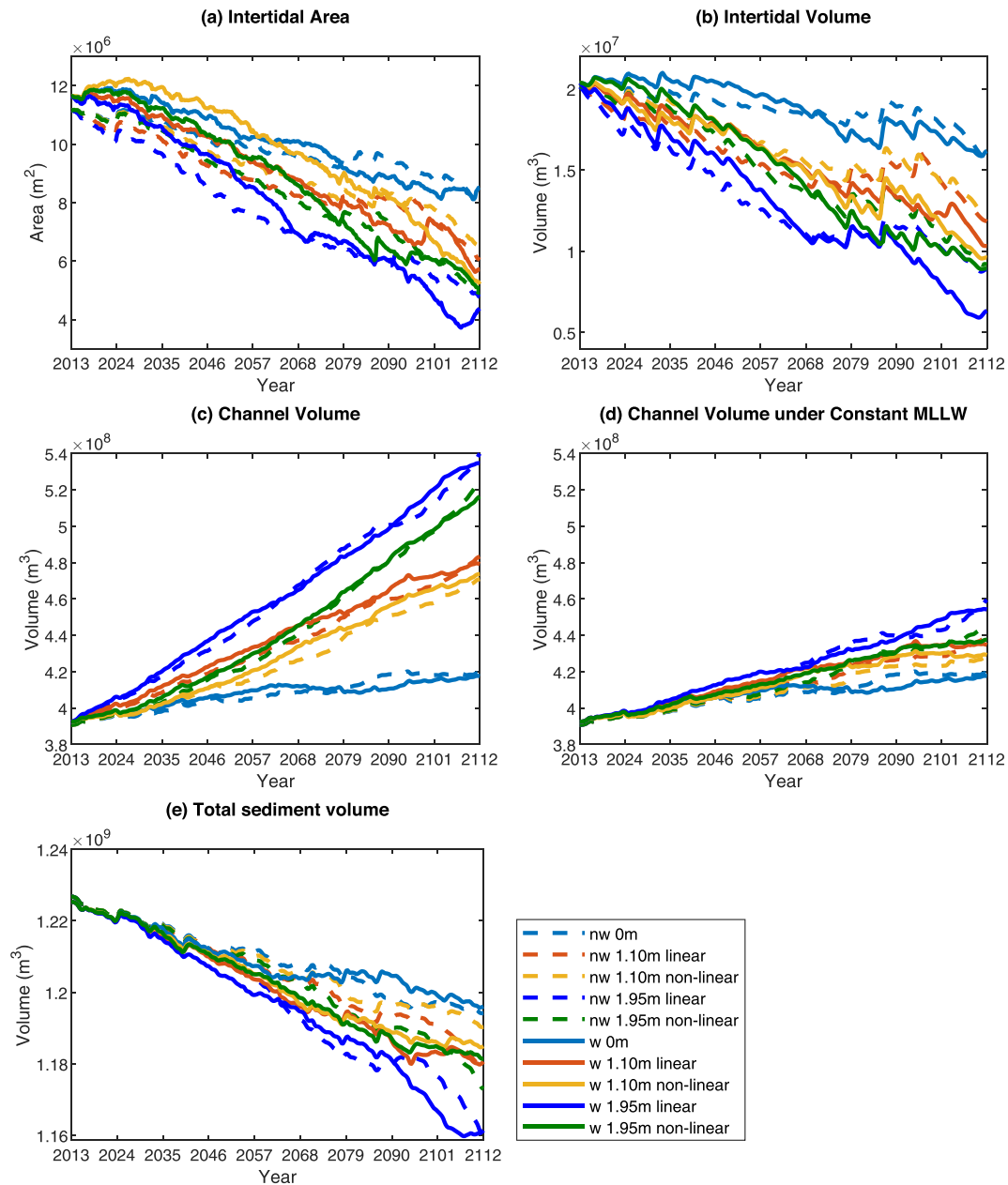


FIGURE 12 Development over 100 years of (a) intertidal area, (b) intertidal volume, (c) channel volume, (d) channel volume under constant mean low low water (MLLW) of NoSLR, and (e) total sediment volume. Dashed lines indicate the NoWave case, while solid lines with the same color indicate the Wave case in the same wind condition. Values are calculated in the study area including Shoal van Ossensisse, the Molenplaat, and the Rug van Baarland. In (a–c), the division between intertidal area and channels is defined based on the averaged MLLW, which is rising with SLR. In (d), the channel volume is calculated under constant MLLW of NoSLR. In (e), total sediment volume is defined above -35 m with respect to constant initial MSL

forcing processes (tidal flow and wind-driven flow). Based on the above, if one focuses on the development of the intertidal flats, wind-waves can be considered as a major driver of morphodynamics, especially in environments with high wave energy and fine sediments.

Wave action on modeled channel–shoal patterns shows some recognized morphological impact. We observe that shoals tend to migrate in the direction of wave propagation, which is consistent with results by DeVet et al. (2018). Furthermore, the larger intertidal area resulting from waves hence leads to channel deepening because of velocity convergence.

Our approach implicitly assumes that developments and interactions with the surroundings of the shoal (i.e., the larger system) are of secondary importance to the processes that we wanted to study

(wind-wave impact and SLR). On a longer timescale, our work shows that wave action does not lead to a fundamentally different morphodynamic behavior. For example, at the end of the hindcast period, the modeled intertidal area under a 207° wind direction accounts for 24% of the total area and differs only 0.6% from the NoWave case, while the channel volume of the Wave case is only 0.14% larger. On the longer timescale of a century, the impact of waves becomes less explicit. Other factors such as tidal asymmetry and tide residual processes start influencing the sediment transport and morphodynamics, making the impact of waves less straightforward to discriminate from other processes.

This suggests that morphodynamic models describing high-resolution wave action on shoals are not required to capture long-

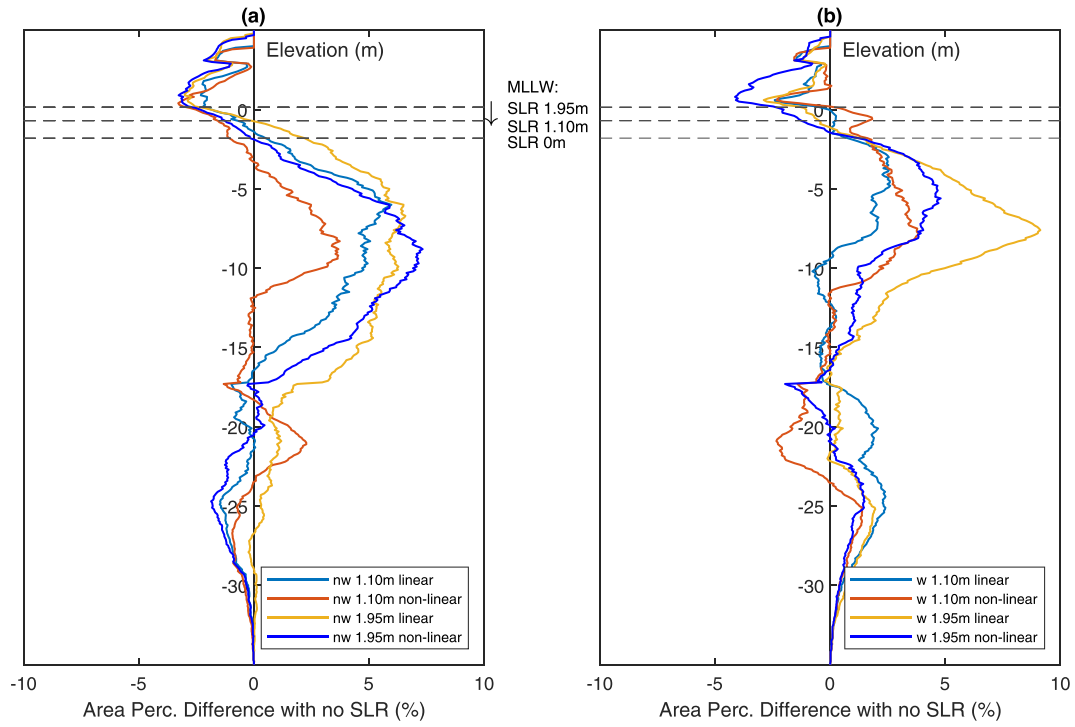


FIGURE 13 (a, b) Area percentage difference between SLR and NoSLR after 100 years in the case of Wave and NoWave, respectively. Positive values imply lower elevation in the case of SLR compared with NoSLR. The vertical axis keeps constant with reference to the initial MSL

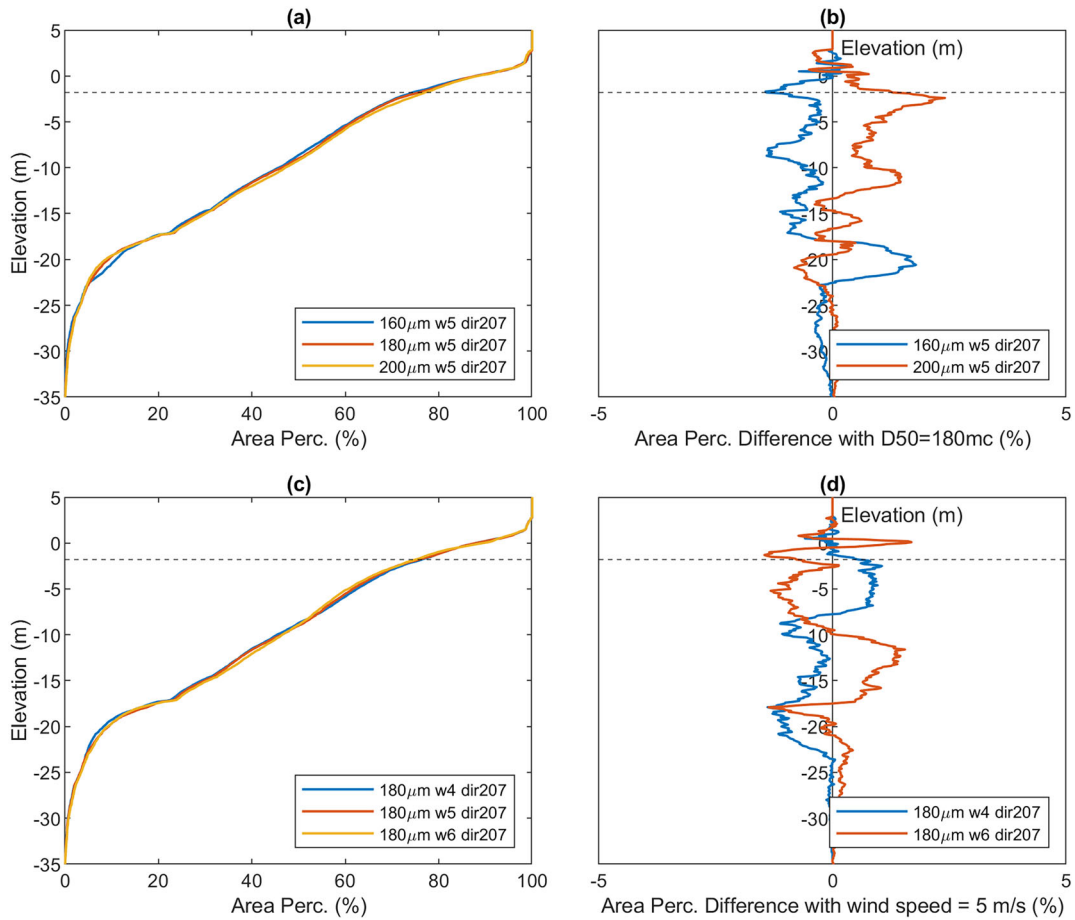


FIGURE 14 Hypsometry after 50 years: (a, b) hypsometry and hypsometric difference with $D_{50}=180 \mu\text{m}$. Positive values imply lower elevation compared with $D_{50}=180 \mu\text{m}$. (c, d): Hypsometry and hypsometric difference with wind speed of 5 m/s. Positive values imply lower elevation compared with wind speed of 5 m/s

TABLE 3 Modeled parameters for the SLR scenarios under wind-waves and after 100 years

Parameters	SLR scenarios		
	0 m	1.10 m linear	1.95 m linear
water depth (m)	0.95	1.68	2.09
Hs (m)	0.06	0.10	0.11
Max. orbital velocity (m/s)	0.04	0.04	0.03
Wave-induced shear stress (N/m ²)	0.34	0.34	0.24
Max. shear stress (N/m ²)	0.80	0.86	0.88

term and large-scale morphodynamic developments of sheltered estuarine systems. This seems to be in contrast with studies by Maan et al. (2015), Van der Wegen et al. (2016), and Elmilady et al. (2019), who suggested that waves are essential for building up shoals and redistributing sediment, especially under SLR scenarios. This may be explained by the fact that they focused on the fringed intertidal area where the shoal of this study is subject to stronger tidal motion. Also, they studied mud flats, while our sediment fraction is sand, which is less sensitive to wave action. In addition, an explanation can be found by tide-residual sediment transport processes that dominate wind-wave processes in building up shoals in environments with limited wave action. Finally, model parameters such as diffusion and viscosity used in low-resolution models may unintentionally include parameterized wave effects. Under these conditions, low-resolution models without wave action could be used in sandy environments if the grid resolution adequately captures the tide-residual sediment transport patterns.

Shoal elevation keeps growing under SLR scenarios, while the amount of intertidal area and volume is not able to keep pace with SLR. This was confirmed by previous numerical model studies (e.g., Dissanayake et al., 2012; Elmilady et al., 2019; Mariotti & Fagherazzi, 2010; Van der Wegen et al., 2016) which showed a notable intertidal area loss caused by the increased inundation despite flat accretion. This also leads to an increased submerged channel volume. In addition, we observe a net erosion in the channel due to SLR. As a combination, a larger channel volume by about 13% and 23% compared with NoSLR arises from 1.10 m and 1.95 m SLR, respectively.

On the long timescale, the impact of waves still influences the sediment redistribution in the estuary, while the impact is minor compared with SLR. After 100 years, the sediment loss due to SLR can be 28.2% more than the total loss of NoSLR for moderate scenarios (1.10 m) and even twice that for extreme scenarios (1.95 m), while the total sediment loss due to waves only fluctuates by less than 18% in all SLR conditions. Table 3 calculates the spatial- and tidal-averaged parameters over Shoal van Ossensisse among different SLR scenarios under wind-waves after 100 years. With the rise of sea level, the averaged water depth increases, resulting in larger significant wave heights due to the longer fetch and less wave dissipation. Despite larger wave height, the averaged maximum orbital velocity and its related wave-induced shear stress drop, since higher water level reduces the probability of waves to feel the bed. However, the maximum shear stress

still observes an increase for the larger SLR scenario, which illustrates that the tidal flow becomes relatively more dominant than wave action. Therefore, the estuary is seen to react more to SLR than waves, and including waves or not does not change the estuarine reaction to SLR. This suggests that, if computational cost is a limitation, the process-based morphodynamic modeling could focus more on the SLR impact than small wind-waves.

7 | CONCLUSIONS

The current research explored the long-term morphodynamic evolution of estuarine sandy shoals under the impact of small wind-waves and sea level rise by means of a numerical, process-based model (Delft3D) in a realistic setting. Firstly, we run models for 50 years, only including wave as a variable. Later, we imposed SLR at the seaward boundary and run models with and without waves under different SLR scenarios for 100 years.

Over the decadal timescale, we observe morphological differences caused by small wind-waves. The estuarine shoals tend to migrate slightly along the direction of wave propagation. The top of the shoal is lowered, with more sediment at shoal edges and downwind side. The channel is wider at larger depths and deeper in the bottom, especially near the areas of wider shoal edges caused by waves.

We investigate the underlying mechanism behind these observed differences. Waves erode the intertidal area by enhancing the bed shear stress on the shoal. The sediment resuspended by waves is partly transported to the leeside of the intertidal area and partly occurs at the shoal edges by ebb currents draining the shoal. As a result, the shoal widens with a decreased channel area. This leads to flow convergence, and deep parts of the channel widen and deepen in response.

However, waves do not lead to a fundamental difference in estuarine evolution. On a long-term timescale, waves keep causing shoal migration in downwind direction and lower the shoal, while the quantitative differences of intertidal area and volume, and channel area and volume diminish or stay constant. On the long-term estuarine scale, small wind-waves are less dominant than the other governed factors that are mainly responsible for the readjustment of channel-shoal patterns, such as tidal asymmetry. The presence of wind-waves does not fundamentally change the general evolution of the estuarine system.

The impact of SLR dominates the effect of wind-waves on the estuarine morphological evolution. The shoal elevation keeps growing with the rising sea level rise, while a notable intertidal area and volume loss still occurs due to the increased inundation. The combination of the increased submerged channel volume and a net channel erosion leads to a larger channel volume caused by SLR. Waves retain the function of lowering the intertidal area and causing channel profile variations, but their impact is limited compared with SLR and the general dynamics of the estuary. The inclusion of waves does not fundamentally change the reaction of the estuary to SLR.

We have different proposals for whether or not to include small wind-waves in the process-based numerical model when studying the estuarine morphology. If one investigates the development of the intertidal flats, we recommend the inclusion of high-resolution small wind-waves on shoals, as wind-waves are major drivers of the intertidal morphodynamics, especially in environments with high wave energy and fine sediment. However, low-resolution models without wave actions could be used to study long-term and large morphodynamic development of a sandy, tide-dominant estuary, if the grid resolution adequately captures the tide-residual sediment transport patterns. The minor impact of wind-waves compared with SLR on the estuarine morphological development on long-term timescales suggests the insignificance of including small wind-waves when investigating anticipated sea level rise scenarios.

Process-based models include many interacting processes and encompass multiple timescales, which makes it difficult to discriminate various impacts. In addition, the extensive dredging activities in the channel and continuous deposition of dredged materials on the shoal may influence the channel profile and disturb the analysis.

This work reveals the significant impact of wind-waves on the morphology of sandy shoals, consistent with literature that studies muddy intertidal flats. Nevertheless, our findings show the minor impact of small wind-waves on a sandy estuarine system as a whole, which is in contrast with some mud studies. Since muddy systems are more sensitive to waves and have different sediment supply sources, they may show distinct behavior. In reality, most estuaries are mixed with sand and mud, thus future research should focus on implementing our approach to a system with multiple sediment fractions.

ACKNOWLEDGEMENTS

The authors acknowledge Rijkswaterstaat and Deltares for funding this research as part of their cooperation with the Flemish Dutch Scheldt Committee.


CONFLICT OF INTERESTS

The authors declare that they have no conflicts of interest to this work. We declare that we do not have any commercial or associative interests that would represent a conflict of interest in connection with the work submitted.

DATA AVAILABILITY STATEMENT

All data presented in this paper are surveyed by Rijkswaterstaat and can be found in the Vaklodingen dataset (<https://publicwiki.deltares.nl/display/OET/Dataset%2Bdocumentation%2BVaklodingen>).

ORCID

- J. Zheng  <https://orcid.org/0000-0001-6186-4740>
 H. Elmilady  <https://orcid.org/0000-0001-9435-0500>
 B.R. Röbbke  <https://orcid.org/0000-0002-2072-8547>
 M. Taal  <https://orcid.org/0000-0001-7669-6049>
 Z.B. Wang  <https://orcid.org/0000-0002-8787-4530>
 B.C. van Prooijen  <https://orcid.org/0000-0003-1375-1498>
 P.L.M. de Vet  <https://orcid.org/0000-0002-7481-8732>
 M. van der Wegen  <https://orcid.org/0000-0002-5227-2679>

REFERENCES

- Ahnert, F. (1960). Estuarine Meanders in the Chesapeake Bay Area. *Geographical Review*, 50(3), 390. <https://doi.org/10.2307/212282>
- Ancora, S., Mariotti, G., Ponchia, R., Fossi, M.C., Leonzio, C. & Bianchi, N. (2020). Trace elements levels in muscle and liver of a rarely investigated large pelagic fish: The Mediterranean spearfish *Tetrapturus belone* (Rafinesque, 1810). *Marine Pollution Bulletin*, 151, 110878. <https://doi.org/10.1016/j.marpolbul.2019.110878>
- Arafat, Y., Pallu, M.S., Maricar, F. & Lopa, R. (2016). Hydrodynamics and morphological changes numerical model of the Jeneberang estuary. *International Journal of Innovative Research in Advanced Engineering (IJIRAE)*, 3(8), 21–29.
- Bearman, J.A., Friedrichs, C.T., Jaffe, B.E. & Foxgrover, A.C. (2010). Spatial trends in tidal flat shape and associated environmental parameters in south San Francisco Bay. *Journal of Coastal Research*, 26(2), 342–349. <https://doi.org/10.2112/08-1094.1>
- Booij, N., Ris, R.C. & Holthuijsen, L.H. (1999). A third-generation wave model for coastal regions 1. Model description and validation. *Journal of Geophysical Research: Oceans*, 104(C4), 7649–7666. <https://doi.org/10.1029/98JC02622>
- Boon, J.D. (1975). Tidal discharge asymmetry in a salt marsh drainage system. *Limnology and Oceanography*, 20(1), 71–80. <https://doi.org/10.4319/lo.1975.20.1.0071>
- Bosboom, J. & Stive, M.J. (2012). Coastal dynamics I: lectures notes CIE4305.
- Braat, L., van Kessel, T., Leuven, J.R. & Kleinhans, M.G. (2017). Effects of mud supply on large-scale estuary morphology and development over centuries to millennia. *Earth Surface Dynamics*, 5(4), 617–652.
- Brown, J.M. & Davies, A.G. (2010). Flood/ebb tidal asymmetry in a shallow sandy estuary and the impact on net sand transport. *Geomorphology*, 114(3), 431–439. <https://doi.org/10.1016/j.geomorph.2009.08.006>
- Christie, M., Dyer, K. & Turner, P. (1999). Sediment flux and bed level measurements from a macro tidal mudflat. *Estuarine, Coastal and Shelf Science*, 49(5), 667–688. <https://doi.org/10.1006/ecss.1999.0525>
- Dam, G. (2013). Actualisatie van het finel2d model van de westerschelde ten behoeve van lange termijn visie scheldeestuarium, veiligheid en toegankelijkheid, Rapport.
- Dam, G., Van der Wegen, M., Labeur, R.J. & Roelvink, D. (2016). Modeling centuries of estuarine morphodynamics in the Western Scheldt estuary. *Geophysical Research Letters*, 43(8), 3839–3847. <https://doi.org/10.1002/2015GL066725>
- de Vet, P.L., van Prooijen, B.C., Colosimo, I., Steiner, N., Ysebaert, T., Herman, P.M. & Wang, Z.B. (2020). Variations in storm-induced bed level dynamics across intertidal flats. *Scientific Reports*, 10(1), 1–15. <https://doi.org/10.1038/s41598-020-69444-7>
- DeVet, P.L., Vanrooijen, B.C., Schrijvershof, R.A., Van der Werf, J.J., Ysebaert, T., Schrijver, M. C. & Wang, Z.B. (2018). The importance of combined tidal and meteorological forces for the flow and sediment transport on intertidal shoals. *Journal of Geophysical Research: Earth Surface*, 123(10), 2464–2480. <https://doi.org/10.1029/2018JF004605>
- Dissanayake, D.M., Ranasinghe, R. & Roelvink, J.A. (2012). The morphological response of large tidal inlet/basin systems to relative sea level rise. *Climatic Change*, 113(2), 253–276. <https://doi.org/10.1007/s10584-012-0402-z>
- Do Ó Martins, A.B., de Assis, A.H.S., Filho, M.S.C., Hatje, V., Moreira, Í.T.A. & de Albergaria-Barbosa, A.C.R. (2020). Concentration and

- distribution of polycyclic aromatic hydrocarbons in oysters from Todos os Santos Bay (Bahia, Brazil). *Marine Pollution Bulletin*, 151, 110781. <https://doi.org/10.1016/j.marpolbul.2019.110781>
- Elmilady, H., Van der Wegen, M., Roelvink, D. & Jaffe, B.E. (2019). Intertidal area disappears under sea level rise: 250 years of morphodynamic modeling in San Pablo Bay, California. *Journal of Geophysical Research: Earth Surface*, 124(1), 38–59. <https://doi.org/10.1029/2018JF004857>
- Elmilady, H., Wegen, M., Roelvink, D. & Spek, A. (2020). Morphodynamic evolution of a fringing sandy shoal: from tidal levees to sea level rise. *Journal of Geophysical Research: Earth Surface*, 125(6), e2019JF005397. <https://doi.org/10.1029/2019JF005397>
- Fagherazzi, S., Palermo, C., Rulli, M. C., Carniello, L. & Defina, A. (2007). Wind waves in shallow microtidal basins and the dynamic equilibrium of tidal flats. *Journal of Geophysical Research: Earth Surface*, 112(2), 1–12. <https://doi.org/10.1029/2006JF000572>
- Friedrichs, C.T. (2012). Tidal Flat Morphodynamics: A Synthesis. In *Treatise on Estuarine and Coastal Science*, Vol. 3; 137–170.
- Galappatti, G. & Vreugdenhil, C. (1985). A depth-integrated model for suspended sediment transport. *Journal of Hydraulic Research*, 23(4), 359–377.
- Ganju, N.K. & Schoellhamer, D.H. (2010). Decadal-timescale estuarine geomorphic change under future scenarios of climate and sediment supply. *Estuaries and Coasts*, 33(1), 15–29. <https://doi.org/10.1007/s12237-009-9244-y>
- Grasmeijer, B., Dam, G. & Taal, M. (2013). Actualisatierapport delft3d schelde-estuarium, Technical (International Marine & Dredging Consultants 2013.
- Hibma, A., Schuttelaars, H. & de Vriend, H. (2004). Initial formation and long-term evolution of channel-shoal patterns. *Continental Shelf Research*, 24(15), 1637–1650. <https://doi.org/10.1016/j.csr.2004.05.003>
- Hunt, S., Bryan, K. R. & Mullarney, J. C. (2015). The influence of wind and waves on the existence of stable intertidal morphology in meso-tidal estuaries. *Geomorphology*, 228: 158–174. <https://doi.org/10.1016/j.geomorph.2014.09.001>
- Janssen-Stelder, B. (2000). The effect of different hydrodynamic conditions on the morphodynamics of a tidal mudflat in the Dutch Wadden Sea. *Continental Shelf Research*, 20(12-13), 1461–1478. [https://doi.org/10.1016/S0278-4343\(00\)00032-7](https://doi.org/10.1016/S0278-4343(00)00032-7)
- Kirby, R. (2000). Practical implications of tidal flat shape. *Continental Shelf Research*, 20(10-11), 1061–1077. [https://doi.org/10.1016/S0278-4343\(00\)00012-1](https://doi.org/10.1016/S0278-4343(00)00012-1)
- Kleinhans, M.G., Jagers, H.R.A., Mosselman, E. & Sloff, C.J. (2008). Bifurcation dynamics and avulsion duration in meandering rivers by one-dimensional and three-dimensional models. *Water Resources Research*, 44(8), 1–31. <https://doi.org/10.1029/2007WR005912>
- Kohsiek, L.H.M., Buist, H.J., Misdorp, R., Berg, J.H. & Visser, J. (1988). Sedimentary processes on a sandy shoal in a mesotidal estuary (Oosterschelde, The Netherlands), Tide-influenced sedimentary environments and facies.
- Kuijper, C., Steijn, R. C., Roelvink, D. & der Kaaij, T.V. (2004). Morphological modelling of the Western Scheldt: validation of DELFT3D. <http://www.vliz.be/en/imis%3Frefid%3D103886>
- Kwon, B.O., Kim, H., Noh, J., Lee, S.Y., Nam, J. & Khim, J.S. (2020). Spatio-temporal variability in microphytobenthic primary production across bare intertidal flat, saltmarsh, and mangrove forest of Asia and Australia. *Marine Pollution Bulletin*, 151: 110707. <https://doi.org/10.1016/j.marpolbul.2019.110707>
- Lanzoni, S. (2002). Long-term evolution and morphodynamic equilibrium of tidal channels. *Journal of Geophysical Research*, 107(C1), 3001. <https://doi.org/10.1029/2000jc000468>
- Le Bars, D., Drijfhout, S. & de Vries, H. (2017). A high-end sea level rise probabilistic projection including rapid Antarctic ice sheet mass loss. *Environmental Research Letters*, 12: 44013. <https://doi.org/10.1088/1748-9326/aa6512>
- Le Hir, P., Roberts, W., Cazaillet, O., Christie, M., Bassoullet, P. & Bacher, C. (2000). Characterization of intertidal flat hydrodynamics. *Continental Shelf Research*, 20(12-13), 1433–1459. [https://doi.org/10.1016/S0278-4343\(00\)00031-5](https://doi.org/10.1016/S0278-4343(00)00031-5)
- Lodder, Q.J., Wang, Z.B., Elias, E.P., Van der Spek, A.J., de Looft, H. & Townend, I.H. (2019). Future response of the Wadden Sea tidal basins to relative sea-level rise—An aggregated modelling approach. *Water*, 11(10), 2198.
- Luan, H.L., Ding, P.X., Wang, Z.B. & Ge, J.Z. (2017). Process-based morphodynamic modeling of the Yangtze Estuary at a decadal timescale: Controls on estuarine evolution and future trends. *Geomorphology*, 290: 347–364. <https://doi.org/10.1016/j.geomorph.2017.04.016>
- Maan, D.C., van Prooijen, B.C., Wang, Z.B. & De Vriend, H.J. (2015). Do intertidal flats ever reach equilibrium? *Journal of Geophysical Research: Earth Surface*, 120(11), 2406–2436. <https://doi.org/10.1002/2014JF003311>
- Maan, D.C., Van Prooijen, B.C., Zhu, Q. & Wang, Z.B. (2018). Morphodynamic feedback loops control stable fringing flats. *Journal of Geophysical Research: Earth Surface*, 123(11), 2993–3012. <https://doi.org/10.1029/2018JF004659>
- Mariotti, G. & Fagherazzi, S. (2010). A numerical model for the coupled long-term evolution of salt marshes and tidal flats. *Journal of Geophysical Research: Earth Surface*, 115(1), 1–15. <https://doi.org/10.1029/2009JF001326>
- Maximova, T., Ides, S., Vanlede, J., De Mulder, T. & Mostaert, F. (2009). Verbetering 2d randvoorwaardenmodel.
- Moyle, P.B., Lund, J.R., Bennett, W.A. & Fleenor, W.E. (2010). Habitat variability and complexity in the upper san francisco estuary. *San Francisco Estuary and Watershed Science*, 8(3), 1–24. <https://doi.org/10.15447/sfews.2010v8iss3art1>
- Nguyen, D., Etri, T., Runte, K.-H. & Mayerle, R. (2011). Morphodynamic modeling of the medium-term migration of a tidal channel using process-based model. *Coastal Engineering Proceedings*, 1(32), 70. <https://doi.org/10.9753/icce.v32.sediment.70>
- Nnafie, A., de Swart, H.E., De Maerschalck, B., Van Oyen, T., van der Vegt, M. & van der Wegen, M. (2019). Closure of secondary basins causes channel deepening in estuaries with moderate to high friction. *Geophysical Research Letters*, 46(22), 13209–13216. <https://doi.org/10.1029/2019GL084444>
- Roberts, W., Le Hir, P. & Whitehouse, R. (2000). Investigation using simple mathematical models of the effect of tidal currents and waves on the profile shape of intertidal mudflats. *Continental Shelf Research*, 20(10-11), 1079–1097. [https://doi.org/10.1016/S0278-4343\(00\)00013-3](https://doi.org/10.1016/S0278-4343(00)00013-3)
- Robinson, A. (1960). Ebb-flood channel systems in sandy bays and estuaries. *Geography*, 45(3), 183–199.
- Schramkowski, G., Schuttelaars, H. & de Swart, H. (2002). The effect of geometry and bottom friction on local bed forms in a tidal embayment. *Continental Shelf Research*, 22(11-13), 1821–1833. [https://doi.org/10.1016/S0278-4343\(02\)00040-7](https://doi.org/10.1016/S0278-4343(02)00040-7)
- Schuttelaars, H.M. & Swart, D.H.E. (1999). Initial formation of channels and shoals in a short tidal embayment. *Journal of Fluid Mechanics*, 386: 15–42. <https://doi.org/10.1017/S0022112099004395>
- Seminara, G. & Tubino, M. (2001). Sand bars in tidal channels. Part 1. Free bars. *Journal of Fluid Mechanics*, 440, 49–74. <https://doi.org/10.1017/S0022112001004748>
- Sutherland, J., Wallingford, H.R., Sutherland, J., Peet, A.H. & Soulsby, R.L. (2075). Evaluating the performance of morphological models Coastal Defence Vulnerability. View project HYDRALAB plus View project Evaluating the performance of morphological models. Elsevier, <https://doi.org/10.1016/j.coastaleng.2004.07.015>
- Van Der Wegen, M. (2013). Numerical modeling of the impact of sea level rise on tidal basin morphodynamics. *Journal of Geophysical Research: Earth Surface*, 118(2), 447–460. <https://doi.org/10.1002/jgrf.20034>
- Van Dijk, W.M., Hiatt, M.R., Van der Werf, J.J. & Kleinhans, M.G. (2019). Effects of shoal margin collapses on the morphodynamics of a sandy estuary. *Journal of Geophysical Research: Earth Surface*, 124(1), 195–215. <https://doi.org/10.1029/2018JF004763>
- Van Goor, M.A., Zitman, T.J., Wang, Z.B. & Stive, M.J. (2003). Impact of sea-level rise on the morphological equilibrium state of tidal inlets. *Marine Geology*, 202(3–4), 211–227. [https://doi.org/10.1016/S0025-3227\(03\)00262-7](https://doi.org/10.1016/S0025-3227(03)00262-7)

- Van Rijn, L.C. (1993). *Principles of sediment transport in rivers, estuaries and coastal seas*, Vol. 1006. Aqua publications Amsterdam: Amsterdam.
- Van Veen, J. (1950). Eb-en vloed-schaar systemen in de Nederlandse getijwateren. *Tijdschrift van het Koninklijk Nederlandsch Aardrijkskundig Genootschap (Ser. 2, 67: 303–350)*.
- Van der Spek, A.J.F. (1994). *Large-scale evolution of Holocene tidal basins in the Netherlands*. Universiteit Utrecht: Faculteit Aardwetenschappen.
- Van der Wegen, M., Jaffe, B., Foxgrover, A. & Roelvink, D. (2016). Mudflat morphodynamics and the impact of sea level rise in South San Francisco Bay. *Estuaries and Coasts*, 40(1), 37–49. <https://doi.org/10.1007/s12237-016-0129-6>
- Van der Wegen, M. & Roelvink, J.A. (2008). Long-term morphodynamic evolution of a tidal embayment using a two-dimensional, process-based model. *Journal of Geophysical Research*, 113(C3), C03016. <https://doi.org/10.1029/2006JC003983>
- Van der Wegen, M. & Roelvink, J.A. (2012). Reproduction of estuarine bathymetry by means of a process-based model: Western Scheldt case study, the Netherlands. *Geomorphology*, 179: 152–167. <https://doi.org/10.1016/j.geomorph.2012.08.007>
- Van der Wegen, M., Roelvink, J.A. & Jaffe, B.E. (2019). Morphodynamic resilience of intertidal mudflats on a seasonal time scale. *Journal of Geophysical Research: Oceans*, 124(11), 8290–8308. <https://doi.org/10.1029/2019JC015492>
- Van der Wegen, M., Van der Werf, J., De vet, L. & Bjorn, R. (2016). Hindcasting Westerschelde morphodynamics (1963–2011). *Deltares Report 1210301-00*.
- Van der Werf, J. & Brière, C. (2013). Influence morphology on tide and sand transport.
- Verlaan, M., De Kleermaeker, S. & Buckman, L. (2015). Glossis: Global storm surge forecasting and information system, Australasian Coasts & Ports Conference 2015: 22nd Australasian Coastal and Ocean Engineering Conference and the 15th Australasian Port and Harbour Conference. Engineers Australia and IPENZ.
- Vroom, J., De Vet, P. & Van der Werf, J. (2015). Validation water movement Delft3D-NeVla model Western Scheldt estuary. *Deltares report*, 1210301–001.
- Vroom, J. & Schrijvershof, R. (2015). Overzicht van menselijke ingrepen in de westerschelde en haar mondingsgebied in de periode 1985–2014. *Deltares memo*, 1210301–001–ZKS–0005 40.
- Wang, Z.B. (1992). Theoretical analysis on depth-integrated modelling of suspended sediment transport. *Journal of Hydraulic Research*, 30(3), 403–421.
- Wang, Z.B., Elias, E. & Briere, C. (2007). Long-term interaction between the Dutch coast and the tidal basins. Z4169.
- Wang, Z.B., Hoekstra, P., Burchard, H., Ridderinkhof, H., De Swart, H.E. & Stive, M.J. (2012). Morphodynamics of the Wadden Sea and its barrier island system. *Ocean and Coastal Management*, 68: 39–57. <https://doi.org/10.1016/j.ocecoaman.2011.12.022>
- Wang, Z.B., Jeuken, M.C., Gerritsen, H., De Vriend, H.J. & Kornman, B.A. (2002). Morphology and asymmetry of the vertical tide in the Westerschelde estuary. *Continental Shelf Research*, 22(17), 2599–2609. [https://doi.org/10.1016/S0278-4343\(02\)00134-6](https://doi.org/10.1016/S0278-4343(02)00134-6)
- Wang, Z.B., Louters, T. & de Vriend, H.J. (1995). Morphodynamic modeling for a tidal inlet in the Wadden Sea. *Marine Geology*, 126(1–4), 289–300. [https://doi.org/10.1016/0025-3227\(95\)00083-B](https://doi.org/10.1016/0025-3227(95)00083-B)
- Yang, S.-L., Friedrichs, C. T., Shi, Z., Ding, P.-X., Zhu, J. & Zhao, Q.-Y. (2003). Morphological response of tidal marshes, flats and channels of the outer Yangtze River mouth to a major storm. *Estuaries*, 26(6), 1416–1425.
- Zhou, Z., Coco, G., Van der Wegen, M., Gong, Z., Zhang, C. & Townend, I. (2015). Modeling sorting dynamics of cohesive and non-cohesive sediments on intertidal flats under the effect of tides and wind waves. *Continental Shelf Research*, 104: 76–91. <https://doi.org/10.1016/j.csr.2015.05.010>

SUPPORTING INFORMATION

Additional supporting information may be found in the online version of the article at the publisher's website.

How to cite this article: Zheng, J., Elmilady, H., Röbbke, B.R., Taal, M., Wang, Z.B., van Prooijen, B.C. et al. (2021) The impact of wind-waves and sea level rise on the morphodynamics of a sandy estuarine shoal. *Earth Surface Processes and Landforms*, 1–18. Available from: <https://doi.org/10.1002/esp.5207>